

DEVELOPMENT OF LOAD DISTRIBUTION MODEL AND  
MICRO-GEOMETRY OPTIMIZATION OF FOUR-POINT CONTACT BALL  
BEARINGS

A THESIS SUBMITTED TO  
THE GRADUATE SCHOOL OF NATURAL AND APPLIED SCIENCES  
OF  
MIDDLE EAST TECHNICAL UNIVERSITY

BY

SİNAN YILMAZ

IN PARTIAL FULFILLMENT OF THE REQUIREMENTS  
FOR  
THE DEGREE OF MASTER OF SCIENCE  
IN  
MECHANICAL ENGINEERING

JUNE 2018



Approval of the thesis:

**DEVELOPMENT OF LOAD DISTRIBUTION MODEL AND  
MICRO-GEOMETRY OPTIMIZATION OF FOUR-POINT CONTACT BALL  
BEARINGS**

submitted by **SİNAN YILMAZ** in partial fulfillment of the requirements for the degree of **Master of Science in Mechanical Engineering Department, Middle East Technical University** by,

Prof. Dr. Halil KALIPÇILAR  
Dean, Graduate School of **Natural and Applied Sciences**

\_\_\_\_\_

Prof. Dr. M.A. Sahir ARIKAN  
Head of Department, **Mechanical Engineering**

\_\_\_\_\_

Prof. Dr. Metin AKKÖK  
Supervisor, **Mechanical Engineering Department, METU**

\_\_\_\_\_

**Examining Committee Members:**

Prof. Dr. F. Suat KADIOĞLU  
Mechanical Engineering Department, METU

\_\_\_\_\_

Prof. Dr. Metin AKKÖK  
Mechanical Engineering Department, METU

\_\_\_\_\_

Prof. Dr. R. Orhan YILDIRIM  
Mechanical Engineering Department, METU

\_\_\_\_\_

Prof. Dr. Ömer ANLAĞAN  
Mechanical Engineering Department, Bilkent University

\_\_\_\_\_

Assist. Prof. Dr. Orkun ÖZŞAHİN  
Mechanical Engineering Department, METU

\_\_\_\_\_

**Date:**

**05.06.2018**

**I hereby declare that all information in this document has been obtained and presented in accordance with academic rules and ethical conduct. I also declare that, as required by these rules and conduct, I have fully cited and referenced all material and results that are not original to this work.**

Name, Last Name: SİNAN YILMAZ

Signature :

## **ABSTRACT**

### **DEVELOPMENT OF LOAD DISTRIBUTION MODEL AND MICRO-GEOMETRY OPTIMIZATION OF FOUR-POINT CONTACT BALL BEARINGS**

YILMAZ, SİNAN

M.S., Department of Mechanical Engineering

Supervisor : Prof. Dr. Metin AKKÖK

June 2018, 82 pages

The unique kinematic characteristics and load-carrying capabilities of four-point contact ball bearings make these bearings being widely used in demanding applications. Particularly, four-point contact ball bearings are preferred due to their reverse axial load carrying capability and high level of stability. In this study, micro and macro geometrical aspects of these bearings are investigated and compared with the conventional ball bearings. Once the geometry and internal kinematics of four-point contact ball bearing are examined and formulated, a comprehensive mathematical model is established to define the load distribution characteristics of four-point contact ball bearings by implementing existing models in literature. The contact between each individual rolling element and raceway are considered in accordance with Hertzian contact theory and formulated with numerical approximation methods. Centrifugal body forces are taken into account in the model in order to capture the behavior of these bearings under high rotational speeds. Moreover, the contact stress and contact truncation formulations are provided for the performance evaluation of four-point contact ball bearings. The developed model is then employed to explore the consistency with the recent FEA studies and software packages under specified load and speed conditions. After the verification of the model, an optimization subroutine is developed in order to optimize the micro-geometry of custom design bearings for

different load and speed conditions as well as for different optimization targets. Several constraints are to be implemented in this optimization subroutine in order not to converge to an infeasible design. Thus, this efficient optimization subroutine is to be a guidance in the design of the custom design bearings for demanding applications. At the end, several optimization results and the corresponding custom design bearing geometries are investigated in terms of the effects of these geometrical parameters on maximum contact stresses, contact truncations and load distributions.

Keywords: Four-point contact ball bearings, split ring ball bearings, optimization of bearing micro-geometry, Hertzian contact theory, bearing load distribution, contact truncation on bearings...

## ÖZ

### **DÖRT NOKTA TEMASLI BİLYELİ RULMANLARIN YÜK DAĞILIM MODELİNİN GELİŞTİRİLMESİ VE MİKRO-GEOMETRİ OPTİMİZASYONU**

YILMAZ, SİNAN

Yüksek Lisans, Makina Mühendisliği Bölümü

Tez Yöneticisi : Prof. Dr. Metin AKKÖK

Haziran 2018 , 82 sayfa

Dört nokta temaslı bilyeli rulmanlar, özgün kinematik karakteristiği ve yük taşıma kapasiteleri nedeniyle kritik uygulamalarda çokça kullanılmaktadır. Özellikle, dört nokta temaslı rulmanlar, ters eksenel yük taşıma kapasiteleri ve sundukları yüksek seviye stabilite nedeniyle tercih edilirler. Bu çalışmada; bu rulman tiplerinin mikro ve makro geometrik özellikleri incelenmiş ve konvansiyonel bilyeli rulmanlarla karşılaştırılmıştır. Dört nokta temaslı bilyeli rulmanların geometrisi ve iç kinematiği formüle edildikten sonra, literatürde yer alan modeller kullanılarak, bu rulmanların yük dağılım karakteristiğini ihtiva eden kapsamlı bir matematik model oluşturulmuştur. Her bir yuvarlanma elamanı ve yuvarlanma yolu arasındaki etkileşim, "Hertz Temas" teorisine bağlı olarak, numerik yakınsama metotları yardımıyla modellenmiştir. Bu rulmanların yüksek dönel hızlardaki davranışlarını saptayabilmek adına, merkezkaç gövde kuvvetleri matematik modelde dikkate alınmıştır. Ayrıca, dört nokta temaslı bilyeli rulmanların performansını değerlendirmek amacıyla, temas gerilme ve temas kesiklik formülasyonları da sağlanmıştır. Kurulan modelin tutarlılığı, belirli yük ve hız koşullarında, yapılan sonlu eleman analizi çalışmaları ve paket bilgisayar programlarıyla karşılaştırılarak kontrol edilmiştir. Matematik modelin tutarlılığı kontrol edildikten sonra, uygulamaya özel rulman mikro geometrisinin, belirli yük ve hız koşullarında ve farklı optimizasyon hedefleri için optimize edilmesini sağlayan bir

optimizasyon kodu geliştirilmiştir. Bu optimizasyon kodunun etkili bir biçimde çalışmasını ve tutarlı bir mikro geometriye yakınsamasını sağlamak amacıyla, çeşitli sınırlamalar eklenmiştir. Böylelikle, geliştirilen optimizasyon kodu uygulamaya özel rulman tasarımında kullanılmak üzere çeşitli kritik uygulamalara rehberlik edecektir. Optimizasyon sonuçları ve ortaya çıkan uygulamaya özel rulman geometrileri göz önünde bulundurularak, rulman geometrik parametrelerin maksimum temas gerilmeleri, temas kesiklikleri ve de yük dağılımı üzerindeki etkileri ele alınmıştır..

Anahtar Kelimeler: Dört nokta temaslı bilyeli rulmanlar, bilezik ayrımlı bilyeli rulmanlar, rulman mikro-geometri optimizasyonu, Hertz temas gerilmesi, rulman yük dağılımı, rulmanlarda temas kesiklikleri...

*To my mother and father and beloved wife...*

## ACKNOWLEDGMENTS

Firstly, I would like to express my sincere gratitude to my supervisor Prof. Metin Akkök for the continuous support of my study and related research, for his patience, motivation, and immense knowledge. His guidance helped me in all the time.

I would like to express my very great appreciation to the very first manager of my career, Zihni Burçay Sarıbay who motivated me to study on the rolling element bearings.

I would also like to extend my thanks to my colleagues in TAI for their support, especially to Dr. Aydın Gündüz for his guidance in studying of the rolling element bearings.

Nobody has been more important to me in the pursuit of this study than the members of my family. I would like to thank my parents, whose love and guidance are with me in whatever I pursue.

Most importantly, I wish to thank my loving and supportive wife, Fatma who has been very patient and encouraged me all the time through this study.

## TABLE OF CONTENTS

ABSTRACT . . . . .	v
ÖZ . . . . .	vii
ACKNOWLEDGMENTS . . . . .	x
TABLE OF CONTENTS . . . . .	xi
LIST OF TABLES . . . . .	xiv
LIST OF FIGURES . . . . .	xv
LIST OF ABBREVIATIONS . . . . .	xvii
LIST OF SYMBOLS . . . . .	xviii
CHAPTERS	
1 INTRODUCTION . . . . .	1
1.1 Motivation of Study . . . . .	4
1.2 Literature Survey . . . . .	6
1.3 Scope of Thesis . . . . .	9
1.4 Outline of Thesis . . . . .	10
2 GEOMETRICAL PARAMETERS OF 4PCBB & APPLICATION OF ELLIPTICAL CONTACT THEORY TO 4PCBB . . . . .	13
2.1 Common Geometrical Parameters of ACBB & 4PCBB . . . . .	13

2.2	Geometrical Parameters of 3PCBB & 4PCBB . . . . .	16
2.3	Elliptical Contact Theory Application to Ball & Raceway Contacts . . . . .	21
3	MATHEMATICAL MODEL FOR THE LOAD DISTRIBUTION OF 4PCBB . . . . .	25
3.1	Comparison with Conventional Ball Bearing Load Distribu- tion Models . . . . .	26
3.2	General Structure of the Mathematical Model of 4PCBB . . .	28
3.3	Kinematics of the Quasi-Static Ball of 4PCBB . . . . .	29
3.4	Ball Equilibrium of 4PCBB under Contact & Body Forces . .	32
3.5	Bearing Reaction Force vs. Applied Ring Load . . . . .	34
3.6	Postprocess for Ellipse Truncation Calculations . . . . .	36
3.7	Results of the Load Distribution Mathematical Model . . . .	38
3.8	Validation of the Model with FEA & CalyX Software . . . .	44
	3.8.1 Comparison with CalyX Software . . . . .	44
	3.8.2 Comparison with Slewing Bearing Simulation Study in ABAQUS . . . . .	48
4	MICRO GEOMETRY OPTIMIZATION OF 4PCBB . . . . .	53
4.1	Optimization Algorithm . . . . .	53
4.2	Fixed Parameters & Design Variables . . . . .	54
4.3	Constraint Implementation and Objective Function of the Op- timization . . . . .	55
4.4	Optimization Results for Selected Bearing and Loading Con- ditions . . . . .	59

4.4.1	Optimization #1: Focusing On Four-Point Contact Avoidance . . . . .	60
4.4.2	Optimization #2: Mainly Focusing on Contact Stress Minimization . . . . .	62
4.4.3	Optimization #3: Focusing on Truncation Avoidance	64
4.5	Summary and Discussions over Optimization Results . . . . .	67
5	CONCLUSIONS & FUTURE WORK . . . . .	71
5.1	Conclusions . . . . .	71
5.2	Outcome of Study & Recommendations for Future Work . . . . .	72
	REFERENCES . . . . .	75
	APPENDICES . . . . .	76
A	COMMAND WINDOWS OF MATLAB DURING OPTIMIZATION	77
A.1	Command Window of MATLAB during Optimization #1 . . . . .	77
A.2	Command Window of MATLAB during Optimization #2 . . . . .	78
A.3	Command Window of MATLAB during Optimization #3 . . . . .	79
B	FLOWCHART OF LOAD DISTRIBUTION MODEL . . . . .	81
B.1	Flowchart of the Mathematical Model for the Load Distribution of 4PCBB . . . . .	82

## LIST OF TABLES

### TABLES

Table 2.1	Coefficients for Exponent, $\lambda$ . . . . .	22
Table 2.2	Coefficients for Approximated Polynomials of Elliptical Integrals . .	22
Table 3.1	Loads for the Results . . . . .	39
Table 3.2	Geometrical Parameters of the Bearing . . . . .	39
Table 3.3	Numerical Comparison with CalyX Results . . . . .	48
Table 3.4	Geometrical Parameters of the Slewing Bearing . . . . .	49
Table 4.1	Fixed Parameters & Design Variables . . . . .	55
Table 4.2	Boundaries for the Design Variables . . . . .	57
Table 4.3	Loads for the Optimization #1 . . . . .	60
Table 4.4	Iterations of Optimization #1 . . . . .	61
Table 4.5	Iterations of Optimization #2 . . . . .	63
Table 4.6	Iterations of Optimization #3 . . . . .	65
Table 4.7	Summary of the Optimizations . . . . .	67
Table 4.8	Optimized Geometrical Parameters . . . . .	68

## LIST OF FIGURES

### FIGURES

Figure 1.1	Four-Point-Contact Ball Bearings with Brass & PEEK Cages . . . .	1
Figure 1.2	Screw Compressor Application of 4PCBB . . . . .	2
Figure 1.3	Wind Turbine Gearbox Application of 4PCBB . . . . .	3
Figure 1.4	4PCBB Slewing Bearing Cross Section . . . . .	3
Figure 1.5	Pinion Shaft of the Helicopter Transmission in AEO Condition . . .	5
Figure 1.6	Pinion Shaft of the Helicopter Transmission in OEI Condition . . .	5
Figure 1.7	Lubrication of 3PCBB between Inner Left and Inner Right Races .	6
Figure 2.1	Basic Geometry of ACBB and Load Carrying Direction . . . . .	14
Figure 2.2	Raceway Curvature Radii and the Distance btw. them . . . . .	15
Figure 2.3	Shim Grinding Operation . . . . .	17
Figure 2.4	Shim Angles under Pure Radial Load . . . . .	17
Figure 2.5	Calculation of the Shim Angles for Inner & Outer Contacts . . . .	18
Figure 2.6	Non-arched Bearing (DGBB) Radial Clearance, $S_d$ . . . . .	19
Figure 2.7	Normalized Internal Clearance Circle . . . . .	20
Figure 3.1	Coordinate System of the Bearing . . . . .	25
Figure 3.2	Ball Numbering and Azimuth Angles . . . . .	26
Figure 3.3	Ball Equilibrium in a Conventional Ball Bearing with Centrifugal Effects i. Not included ii. Included . . . . .	27
Figure 3.4	Ball and Raceway Centers at Initial and Deformed Positions . . . .	30
Figure 3.5	Ball at Equilibrium Condition . . . . .	33

Figure 3.6	Ellipse Truncation . . . . .	37
Figure 3.7	Contact ellipse at the loaded contact angle . . . . .	37
Figure 3.8	Results for Load A . . . . .	41
Figure 3.9	Results for Load B . . . . .	42
Figure 3.10	Results for Load C . . . . .	43
Figure 3.11	CalyX Gearbox Model for Validation . . . . .	44
Figure 3.12	Simulation Results on Meshed Model . . . . .	45
Figure 3.13	CalyX Load Distribution with Reaction Force . . . . .	46
Figure 3.14	CalyX Maximum Contact Stress Distribution with Reaction Force . . . . .	46
Figure 3.15	Contact Load Comparison of Calyx and MATLAB Model . . . . .	47
Figure 3.16	Model of the Contact . . . . .	49
Figure 3.17	FE Model of the Slewing Bearing . . . . .	50
Figure 3.18	Load Distribution of the Slewing Bearing . . . . .	51
Figure 3.19	Load Distribution Comparison of FEA and MATLAB Models . . . . .	52
Figure 4.1	Objective Functions at Each Iteration of Optimization #1 . . . . .	61
Figure 4.2	Contact Stress Distribution for Initial & Optimized Design of Optimization #1 . . . . .	62
Figure 4.3	Objective Functions at Each Iteration of Optimization #2 . . . . .	63
Figure 4.4	Contact Stress Distributions for Initial & Optimized Design of Optimization #2 . . . . .	64
Figure 4.5	Objective Functions at Each Iteration of Optimization #3 . . . . .	65
Figure 4.6	Contact Stress Distributions for Initial & Optimized Design of Optimization #3 . . . . .	66
Figure 4.7	Truncation Distributions for Initial & Optimized Design of Optimization #3 . . . . .	66

## **LIST OF ABBREVIATIONS**

3PCBB	Three-Point-Contact Ball Bearing
4PCBB	Four-Point-Contact Ball Bearing
ACBB	Angular Contact Ball Bearing
AEO	All Engine Operative
DGBB	Deep Groove Ball Bearing
DoF	Degrees of Freedom
FE	Finite Element
FEA	Finite Element Analysis
OEI	One Engine Inoperative

## LIST OF SYMBOLS

$a$	Semi-major axes of the contact ellipse
$b$	Semi-minor axes of the contact ellipse
$B$	Total curvature of bearing
$d_m$	Pitch diameter
$D$	Ball diameter
$D_i$	Bore diameter
$D_o$	Outer diameter
$D_s$	Shoulder diameter
$E$	Elastic modulus
$\mathcal{E}$	Elliptical integral of second kind
$\mathcal{F}$	Elliptical integral of first kind
$f$	Osculation, conformity of raceway
$[F]$	Ring Load Matrix
$F_c$	Centrifugal force
$g$	Shim thickness (raceway curvature center distance)
$H_s$	Shoulder to raceway center vertical distance
$K$	Contact stiffness
$n$	Rotational speed in rpm
$P$	Optimization penalty function
$P_d$	Radial play of arched bearing
$P_e$	Axial play of arched bearing
$Q$	Contact load
$r$	Raceway curvature radius
$R_i$	Bearing axis to inner raceway center distance
$R_o$	Bearing axis to outer raceway center distance
$S_d$	Radial play of non-arched bearing
$St$	Shoulder thickness
$TR$	Ellipse truncation in percentage
$Z$	Number of balls

## **Greek Letters**

$\alpha_0$	Unloaded contact angle
$\alpha$	Loaded contact angle
$\alpha_s$	Shim (resting) angle
$\delta$	Contact deflection
$[\delta]$	Ring Deflection Matrix
$\theta_s$	Shoulder edge angle
$\kappa$	Ellipticity parameter
$\nu$	Poisson's ratio
$\omega$	Rotational speed
$\phi$	Non-constrained objective function of optimization
$\phi_c$	Constrained objective function of optimization
$\Psi$	Azimuth (index) angle
$\sigma$	Maximum contact stress
$\Sigma\rho$	Curvature sum
$F\rho$	Curvature difference

## **Subscripts**

$m = i, o$	Inner and Outer
$k = l, r$	Left and Right
$j = 1, 2, \dots, Z$	Ball Number

## **Operators**

$SGN$	Sign Function $SGN(-) = -1, SGN(+) = 1$
-------	---



## CHAPTER 1

### INTRODUCTION

In today's industry, rolling-element bearings are still irreplaceable by means of efficiency, service interval, reliability, size, weight and cost. While much more demanding applications for rolling element bearings are evolving, today's advanced manufacturing, engineering and computer tools make it possible to generate solutions to these applications. Four-point contact ball bearing (4PCBB) is one of those solutions for special applications with its unique geometry which is able to contain high contact angles in both axial directions with relatively low axial clearance.



Figure 1.1: Four-Point Contact Ball Bearings with Brass & PEEK Cages [1]

Four-point contact ball bearing (4PCBB) is an excellent choice for the applications which require the accommodation of the axial loads in both directions. By this

characteristic, it is possible to eliminate one row of a bearing in particular applications. In this way, weight, space and cost savings are achieved by employing these bearings. Therefore, 4PCBBs are suitable for the designs where space limitations exist with high axial loads in both directions or with high speeds. Moreover, these bearings are capable of positioning the shafts with very close tolerances due to their low axial clearance. Thus, 4PCBBs are widely used in the applications such as pumps, retarders, compressors, industrial or automotive gearboxes as well as the helicopter gearboxes.

For example, in Figure 1.2, screw compressor with two helical screws are supported by the 4PCBBs. Since the narrow gaps between these two screws as well as the housings are crucial for the proper operation, 4PCBBs are utilized with their low axial clearance to provide a stiff axial arrangement.

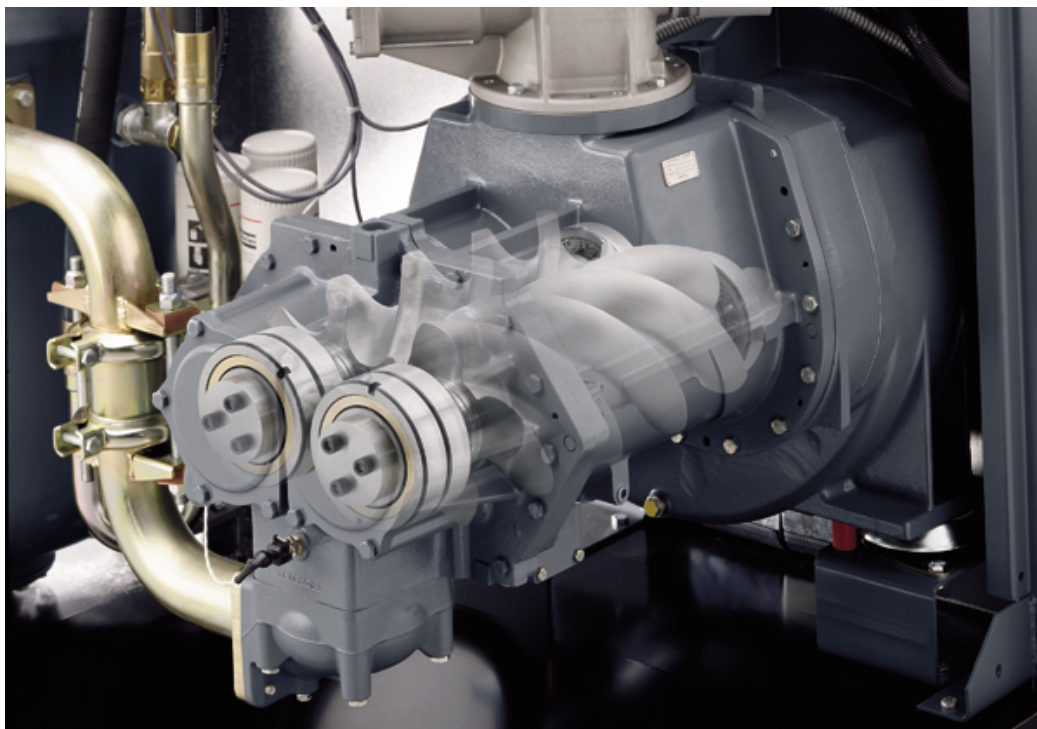


Figure 1.2: Screw Compressor Application of 4PCBB [1]

In the wind turbine gearbox example shown in Figure 1.3, the high speed shaft of the gearbox is configured to have 4PCBB combined with the cylindrical roller bearing in order to accommodate the heavy axial loads caused by the helical gear mesh.

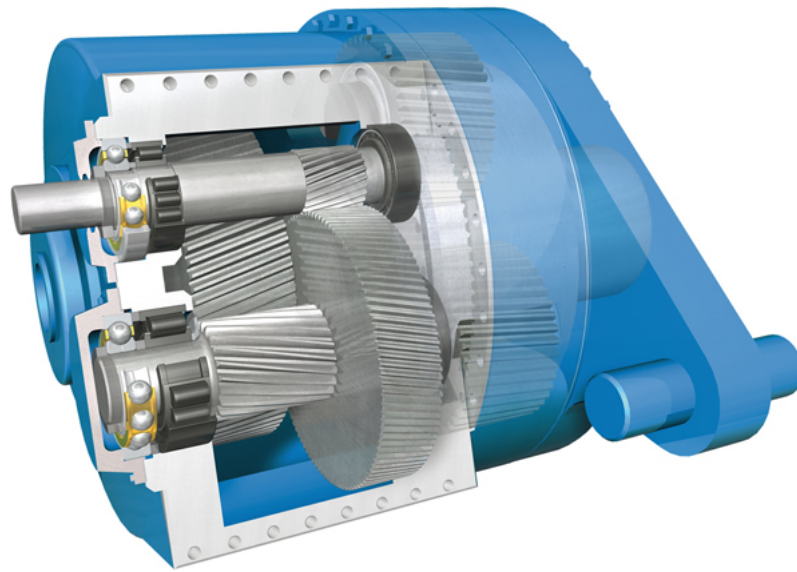


Figure 1.3: Wind Turbine Gearbox Application of 4PCBB [1]

4PCBBs in large diameters (Figure 1.4) are also used as slewing bearing which typically supports a heavy but slow-turning or slow-oscillating load, often in a horizontal platform such as a conventional crane, a swing yarder, or the wind-facing platform of a horizontal-axis windmill.

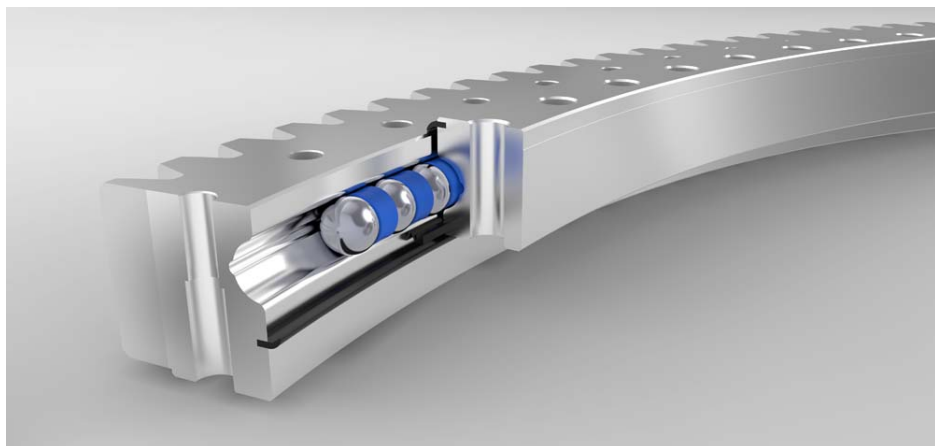


Figure 1.4: 4PCBB Slewing Bearing Cross Section [2]

## 1.1 Motivation of Study

Four-point contact ball bearings are also called as split race ball bearings. Splitting the races is only because of the manufacturing and/or assembly purposes. There are two options for 4PCBBs to be manufactured. First method is to splitting the races as left and right for both inner and outer races. After splitting, the shim grinding operation is carried out between two faces of the left and right races in order to have a 4PCBB. Second method is to grind with special grinding technique called "Gothic Arched Grinding". In this method, it is not required to split the races in order to have 4PCBB configuration within the bearing. Before shim grinding operation and separation of the rings, these bearings are simply like a deep groove ball bearing (DGBB). If gothic arched grinding or shim grinding is made for only one ring (inner or outer), this makes the bearing have a three-point contact ball bearing (3PCBB) configuration.

The unique characteristics of these bearings make them efficient solutions for special cases. The major benefit of the 3PCBBs or 4PCBBs is the capacity of carrying reverse axial load. In other words, these bearing have high axial load carrying capacity in both axial directions. Therefore, in some cases, this specific feature may remove the need of one more row of a bearing in a shaft-bearing system. In order to give an example for this, pinion shaft of a helicopter transmission can be taken as a case study. In the twin-engine helicopters, there exist flight conditions such as: All Engine Operative (AEO) or One Engine Inoperative (OEI). The pinion shafts which are driven by each engine, are meshed with the collector gear to unite the total power and to transmit to the rotors. In the case of a failure in the one of the engines, i.e. in OEI condition, the other engine is capable to maintain the flight. However, since the pinion shaft, which is connected to the failed engine, will be the driven member but not the driver any more, in the OEI case, the axial load on the pinion shaft will be reversed. Therefore, it is required for these pinion shafts to be designed such that they could carry the axial loads in both direction.

In Figure 1.5, it is seen that there are three rows of bearings (ACBB-1, ACBB-2 and 4PCBB) which share the total axial load that is in the -Z direction. However, in the OEI flight condition, the axial load is reversed to +Z direction as in the Figure 1.6. Conventional angular contact ball bearings (ACBB) can carry the axial load in only

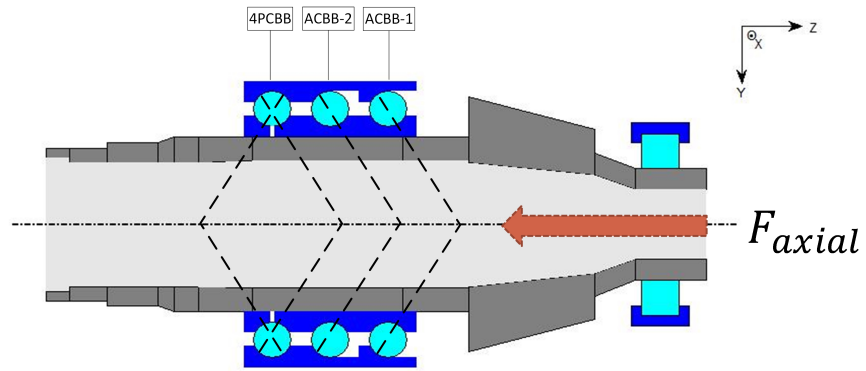


Figure 1.5: Pinion Shaft of the Helicopter Transmission in AEO Condition

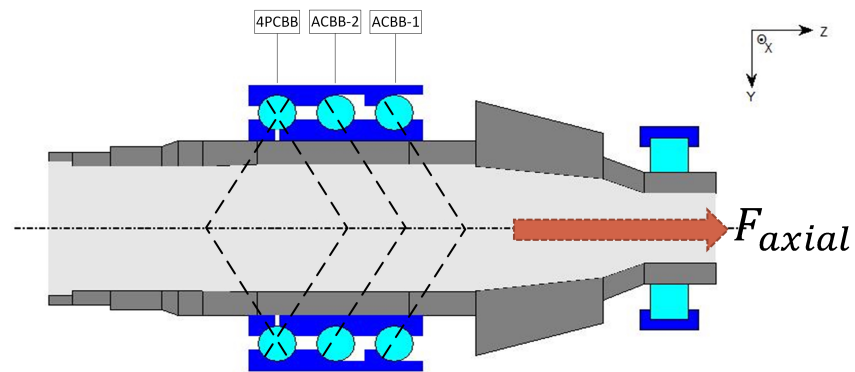


Figure 1.6: Pinion Shaft of the Helicopter Transmission in OEI Condition

one direction. Therefore, in OEI case, all the axial load is carried by the 4PCBB. By employing this 4PCBB, they are both guaranteed to increase the axial load carrying capacity in  $-Z$  direction in AEO case and to support the shaft  $+Z$  direction in OEI case.

Another unique difference of 3PCBBs and 4PCBBs from ACBBs is the axial end-play which is simply the axial clearance of the bearings. In the operation, this clearance diminishes and the rolling elements get in contact with both inner and outer rings. In some cases, in a gearbox, it is needed to limit the axial end-play of the shafts. In these cases, the 3PCBBs and the 4PCBBs would be the solution. When it is compared for the axial end-play:  $ACBB > 3PCBB > 4PCBB$  for the bearings with equal geometry.

In addition to, these bearing concepts have specific advantages in special conditions which require assembly easiness with split races. Also, with split races or with gothic arched design it is possible to provide much more efficient lubrication to the contact zones as given in Figure 1.7.

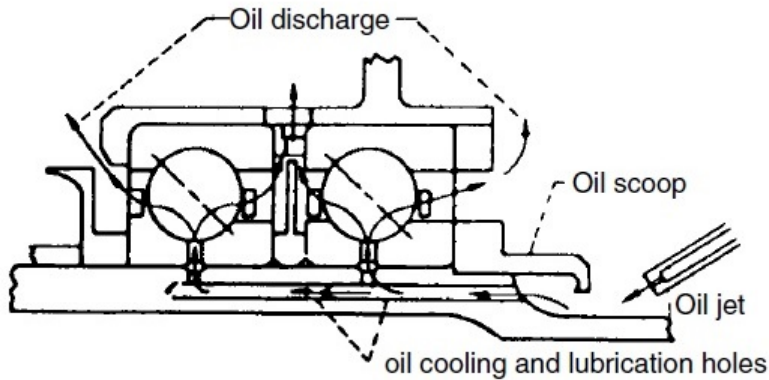


Figure 1.7: Lubrication of 3PCBB between Inner Left and Inner Right Races [3]

To summarize, 3PCBBs and 4PCBBs have unique advantages with their special design. However, despite their names, these bearings shall be operated as conventional ACBBs in the normal operation. In other words, these bearings shall not have three- or four-point contact in any of the rolling elements because of the risk of excessive heat generation and premature failure which results from the three- or four- point contact. Therefore, the design and the optimization of these bearings carry great importance in order to guarantee safe and efficient operation of the gearboxes. This study might be a guidance for the designers by generating an optimization subroutine which forms the optimal bearing geometry for a specific operation and condition.

## 1.2 Literature Survey

In order to establish an efficient mathematical model for the load distribution of 4PCBB, it is required to analyze the existing models starting with the conventional ball bearing theory.

Bearing theories which generate the bearing load-deflection relationships, consist the contact mechanics between rolling elements and the raceways. Therefore, the

Hertzian contact theory is the foundation of the bearing theories. Hertzian contact theory is studied and used in plenty of textbooks and handbooks. To illustrate, Harris [3] summed up and formulate Hertz contact on bearings. Furthermore, in the ISO16281 [4], the Hertzian contact theory and application to ball and roller bearings is explained briefly. Antoine et al. [5], developed an approximate analytical model for Hertzian contact theory of the elliptical contacts and confronted with the studies in the literature. These studies on Hertzian contact theory have been implemented in the rolling-element bearings' mathematical models in order to simulate the interaction between rolling elements and raceways by contact stiffness. For the roller bearings, the line contact mechanics and laminae models are developed to generate load-deflection relationship within the bearing. For the ball bearings which is also the scope of this study, nature of the ball and raceway interaction results an elliptical point contact.

The one of the earliest and the most comprehensive study on the ball bearings is developed by Jones [6]. In this study, a completely general solution is obtained, whereby the elastic compliances of a system of any number of ball and radial roller bearings under any system of loads can be determined. Gyroscopic forces and moments acting on the bearing rolling elements are also included in order to capture the dynamic effects of high-speed operation. That study of Jones [6] is referenced in many other studies in rolling-element bearing literature. In that study, the bearing rings are assumed to be rigid. Elastic deformations are only said to be in contact zones. This assumption is very appropriate for most of the bearing applications. Moreover, Harris and Broschard [7] extended the studies with taking into consideration the structural deformation of the outer ring with an elliptical inner ring in order to capture the ring deformation effects which carry great importance in the analysis of planetary gear bearing applications.

On the theory of ball bearings, there exist other studies focusing on the different parameters and phenomena. De Mul et al. [8] generated a mathematical model in order to simulate the bearing equilibrium and associated load distribution in five degrees of freedom. In that study, ball contact stiffness matrix is developed both with and without ball centrifugal loads. Also, Lim et al. [9] focused on the bearing stiffness matrix which is an important parameter for vibratory motion from the rotating shafts

to the flexible or rigid casings through rolling-element bearings. Hernot et al. [10] calculated the angular contact ball bearing stiffness matrix analytically by replacing the summation of ball-race loads by an integration. These advanced studies are simplified and summarized in ISO16281 [4] in order to guide for calculation of the load distribution within the rolling elements of an axially and radially loaded ball bearing by ignoring the gyroscopic effects. In that model, the formulation is given for bearing loading in three degrees of freedom which are two translational (axial and radial load) and one rotational (radial moment). Also in ISO16281 [4], established basic load distribution model is used for the calculation of the basic and modified reference rating life.

Previously, the studies that are focused on the conventional ball bearings are mentioned. These studies are important guidance in the development of 3PCBB & 4PCBB models. The very first analysis of the arched ball bearing is made by Hamrock and Anderson [11]. The model of axially loaded arched outer-race ball bearing with only centrifugal loads was developed in that study. Furthermore, Hamrock [12] improved the model by adding gyroscopic moment and friction. With the enhanced calculation power of the advanced computer tools, more recently, studies on the 3PCBB & 4PCBB have evolved in order to model the bearings under complex loading and high speed conditions. Amasorrain et al. [13] established a model for load distribution of four-point contact slewing ball bearing under three degrees of freedom loading condition (radial load, axial load & radial moment). In that study, the gyroscopic effects were neglected since these slewing bearings are used in applications such as tower cranes, wind-power generators, excavation machinery which are running at relatively low speeds. Leblanc and Nelias [14] extended this work to a five degrees of freedom system with also including the gyroscopic effects, friction and film thickness. Moreover, Halpin and Tran [15] proposed an analytical model for load distribution of 4PCBB. In that model race control theory is replaced with a minimum energy state theory to allow both spin and slip to occur at the ball-to-raceway contact. However, that model neglects the effects from gyroscopic moments and only considers the dynamic body forces from centrifugal effects. Recently, Liu et al. [16] simulate the slewing bearing by modelling the balls under compression with traction-only non-linear springs and validated the resultant load distribution with the experimental

results.

In conclusion, these studies and models are focusing different key parameters of the 3PCBB & 4PCBB for different applications. The assumptions, geometrical & loading considerations, simulation costs etc. shall be established carefully for each unique application.

### **1.3 Scope of Thesis**

In this study, it is aimed to develop and/or to modify the most reasonable mathematical model in order to make it possible for the optimization of micro-geometry of the 4PCBB for a specific application. For this purpose, developed bearing model is explained in terms of the assumptions, considerations that is required for an efficient optimization subroutine.

In order to develop the mathematical model for load distribution of 4PCBB, the models that exist in literature are investigated and formulated. The established model is formulated in MATLAB environment in order to benefit the existing MATLAB functions and solvers. The model is to be verified with the existing studies. Moreover, the model is used for obtaining the internal load distribution, contact stresses, contact deflections and loaded contact angles under a prescribed load and speed conditions.

Generated model is to be employed under an optimization subroutine in order to make it possible to automate micro-geometry optimization of the custom design bearings. In this optimization subroutine, the bearing macro-geometry and the operational conditions are pre-determined depending on the application. Objective of the optimization is to find the optimum micro-geometry for a minimum contact stress. Furthermore, the ellipse truncation phenomenon as well as avoiding the possible three- or four-point contact in any of the rolling element are taken into account. The other geometrical and manufacturability constraints are to be defined at the beginning of the optimization in order not to optimize for an infeasible design.

Finally, the established model is to be used for different macro & micro geometries as well as different loading conditions to sense the behaviour of the 4PCBBs and

possible reasons for the rolling elements to be loaded more than two points.

## **1.4 Outline of Thesis**

This study contains five main chapters. The first chapter is the introduction of the study in terms of motivation, literature background of the problem and scope of the study.

In Chapter 2, ball bearing geometry and the contact theory is summarized. The differences between the 4PCBBs and conventional ACBBs in terms of geometrical parameters are given in Chapter 2. In addition to, the geometrical parameters unique to 4PCBBs are also introduced. The contact theory that is needed for generating the deflection and the load relation for a specific raceway to ball contact is also given in Chapter 2. For this purpose, study of [5] is summarized and applied to ball & raceway contact. In this study, the Hertzian contact theory is approximated by a numerical solution which gives good precision with respect to analytical solution. Moreover, the contact stress calculations are presented in Chapter 2.

In Chapter 3, the coordinate system, and ball indexing are introduced. The differences between the kinematics of ACBBs and 4PCBBs are also summarized. General structure of the mathematical model for the load distribution of 4PCBB is given. The input and output parameters are also introduced. Kinematics of a quasi-static ball is briefly explained in Chapter 3. The formulation based on this kinematics as well as the force equilibrium on a single ball are presented. The constraint equations that relate the applied ring loads to bearing reaction forces are given in Chapter 3. Moreover, the post-process calculations which include the ellipse truncation phenomenon are shown. The sample results of the established model are given for different load conditions. Validation and comparison with FEA studies and other software packages are introduced in Chapter 3.

In Chapter 4, micro-geometry optimization subroutine of the custom design 4PCBB is established. For this purpose, the optimization parameters as well as the constraints that ensure the feasibility of the optimization are introduced. Non-constrained and constrained objective functions are built in Chapter 4. The results and summary of

the optimization for different cases as well as the discussions over those results are given at the end of Chapter 3.

In Chapter 5, discussions are given in terms of the assumptions within the generated model and the corresponding results. Furthermore, the outcomes of the study and possible future works are presented in Chapter 5.



## CHAPTER 2

### GEOMETRICAL PARAMETERS OF 4PCBB & APPLICATION OF ELLIPTICAL CONTACT THEORY TO 4PCBB

Rolling contact bearings are seemed like basic mechanisms. In fact, there exist plenty of geometrical parameters within these bearings. These parameters are very effective on the bearing performance like contact stress, load carrying capacity, basic life and lubrication factors. In this chapter these geometrical parameters of ball bearings are presented. Also, the differences and similarities of ACBBs and 4PCBB in terms of geometry are stated.

#### 2.1 Common Geometrical Parameters of ACBB & 4PCBB

In this section, the geometry of the conventional ACBBs are focused on. Since ACBBs and 4PCBBs have some common geometrical parameters, they are explained in this section. However, differences between ACBBs and 4PCBBs in terms of geometrical parameters are stated in Section 2.2.

As seen on the Figure 2.1, ACBBs have basic geometrical parameters such as the diameters where the bearing is mounted on the shafts (Bore Diameter,  $D_i$ ) and housings (Outer Diameter,  $D_o$ ). Balls with diameter,  $D$  are rolling in the orbital diameter called: pitch diameter,  $d_m$ . The race designs with corresponding micro geometries, incorporate the contact angle,  $\alpha$  which is an important parameter in the axial load carrying direction and capacity. Also, as given in Figure 2.1, shown bearing is capable of carrying the axial load applied to the shaft in the shown direction by the nature of its design.

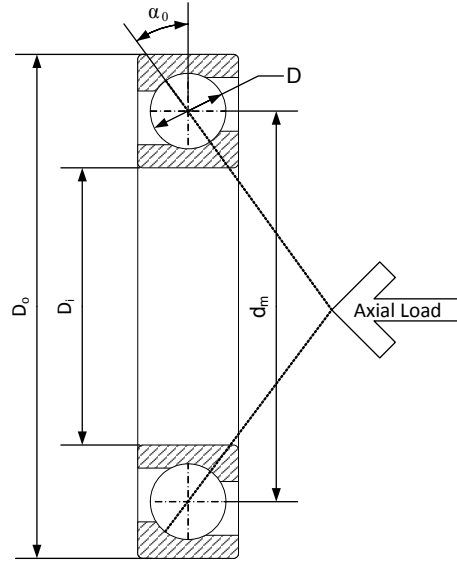


Figure 2.1: Basic Geometry of ACBB and Load Carrying Direction

Some parameters that are shown on the Figure 2.1 are becoming dummy in the mathematical model of the ACBBs. For example, the diameters  $D_o$ ,  $D_i$  are ineffective and not included in the models due to the assumption of rigid rings and elastic deformation only at contact points. However, for the most of the bearings, Equation 2.1 can be taken as a reference to estimate the pitch diameter,  $d_m$ .

$$d_m \approx \frac{1}{2}(D_o + D_i) \quad (2.1)$$

The radial ball bearings, in other words; Deep Groove Ball Bearings (DGBB) carry an internal clearance called diametral clearance or radial clearance in their internal design. However, In ACBBs this clearance diminishes when they mounted into a system. Instead of this clearance, ACBB has a mounted contact angle i.e. unloaded contact angle,  $\alpha_0$ . In the study [17], a comprehensive analysis on the effects of clearance on the conventional bearings are presented.

Raceway radii define the load carrying ability of a bearing with the other parameters. Inner and outer raceway radii,  $r_i$  &  $r_o$  are generally slightly larger than the ball radius. In order to, give the sense of the measure between ball diameters and the raceway radii, the definition osculation,  $f$  is used. As given in Equation 2.2, osculation is

simply the ratio of the raceway radius to ball diameter.

$$f = r/D \tag{2.2}$$

In Figure 2.2, the distance between the centers of the raceway curvature radii is shown as  $A_0$ . The relation between these parameters are given in Equation 2.3.

$$A_0 = r_i + r_o - D \tag{2.3}$$

$$A_0 = (f_i + f_o - 1)D = BD \tag{2.4}$$

By substituting Equation 2.2 to Equation 2.3, the total curvature of the bearing,  $B = f_i + f_o - 1$  is obtained as in Equation 2.4.

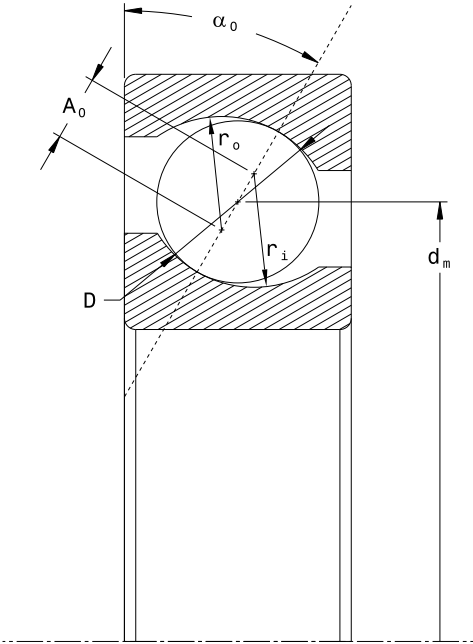


Figure 2.2: Raceway Curvature Radii and the Distance btw. them

In order to establish the contact stiffness between raceways and the rolling elements in Section 2.3, it is required to calculate the necessary contact parameters such as: the curvature sum,  $\Sigma\rho$  and the curvature difference,  $F(\rho)$ . These parameters are briefly explained by Harris [3]. Basically, for inner raceway and the ball contact, curvature

sum and curvature difference become;

$$\Sigma\rho_i = \frac{1}{D} \left( 4 - \frac{1}{f_i} + \frac{2\gamma}{1-\gamma} \right) \text{ and} \quad (2.5)$$

$$F(\rho)_i = \frac{\frac{1}{f_i} + \frac{2\gamma}{1-\gamma}}{4 - \frac{1}{f_i} + \frac{2\gamma}{1-\gamma}}, \text{ respectively.} \quad (2.6)$$

Similarly for the outer raceway and the ball contact;

$$\Sigma\rho_o = \frac{1}{D} \left( 4 - \frac{1}{f_o} - \frac{2\gamma}{1+\gamma} \right) \text{ and} \quad (2.7)$$

$$F(\rho)_o = \frac{\frac{1}{f_o} - \frac{2\gamma}{1+\gamma}}{4 - \frac{1}{f_o} - \frac{2\gamma}{1+\gamma}}, \text{ respectively.} \quad (2.8)$$

$$\text{Where; } \gamma = \frac{D \cos \alpha}{d_m}. \quad (2.9)$$

The parameter  $\alpha$  is the loaded contact angle which is specific for each rolling element and for each raceway contact. Therefore, in the following sections where the mathematical model is established, subscripts will be added on the parameters such as loaded contact angle, in order to identify the overall kinematics of the bearing.

## 2.2 Geometrical Parameters of 3PCBB & 4PCBB

3PCBBs & 4PCBBs have some unique geometrical parameters which make these bearings efficient in terms of reverse axial load carrying capacity. These bearings are also called as split ring bearings depending on which ring the shim grinding operation is made. In Figure 2.3 the shim grinding operation is illustrated. The two inner rings (left & right) are ground on the mating surfaces by an equal length of  $g_i/2$ . This operation makes the raceway curvature radii centers to be separated by the dimension of  $g_i$  (raceway curvature center distance). If this operation is carried out for only inner

or outer rings, this makes bearing to be a 3PCBB. For the case where shim grinding operation is done for both inner & outer rings, the bearing becomes a 4PCBB.

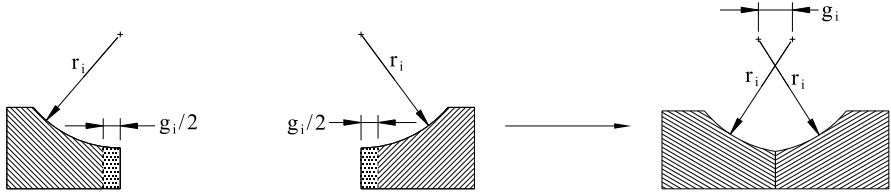


Figure 2.3: Shim Grinding Operation

Shim grinding operation transforms a DGBB into a 3PCBB or 4PCBB. While doing this, some geometrical parameters are generated or altered. The shim grinding operation and the separation of the raceway curvature centers make bearing to form possible four point contacts under pure radial load which are oriented as in Figure 2.4.

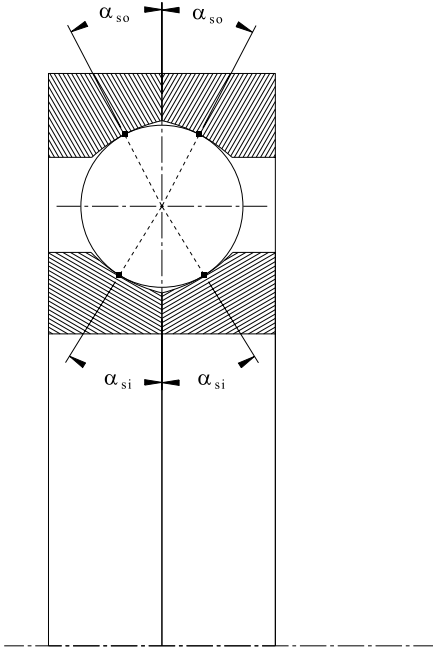


Figure 2.4: Shim Angles under Pure Radial Load

The shown angles are called as the shim angle or the resting angle. Since the shim grinding for left and right rings are assumed to be equal, the shim angles are also equal for left and right contacts. The shim angles for inner and outer contacts,  $\alpha_{si}$  and  $\alpha_{so}$  are calculated with respect to the Figure 2.5. These shim angles for inner and

outer contacts are given in Equation 2.10 & 2.11, respectively.

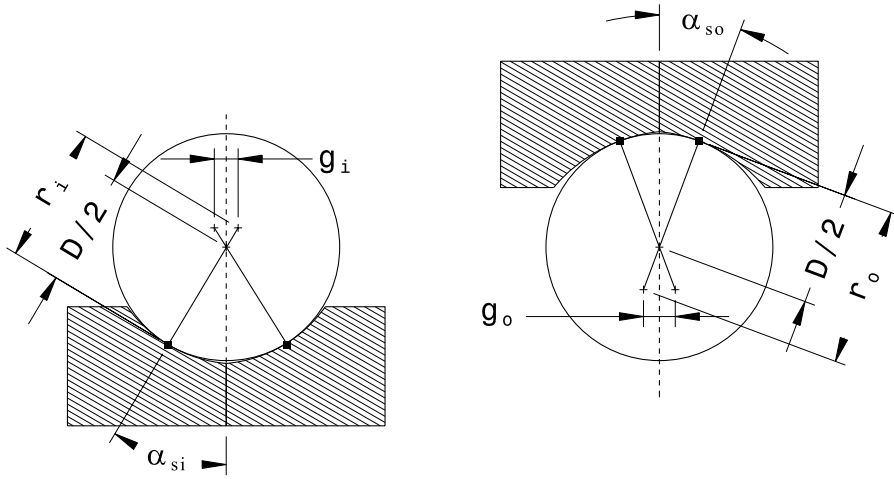


Figure 2.5: Calculation of the Shim Angles for Inner & Outer Contacts

$$\alpha_{si} = \sin^{-1} \left( \frac{g_i}{2r_i - D} \right) \quad (2.10)$$

$$\alpha_{so} = \sin^{-1} \left( \frac{g_o}{2r_o - D} \right) \quad (2.11)$$

The non-arched bearing radial clearance,  $S_d$  is illustrated in Figure 2.6. The non-arched bearing radial play,  $S_d$  is changed to the arched or 4PCBB bearing radial play,  $P_d$  with shim grinding or gothic arched grinding. Since the raceway curvature centers are separated, the rolling elements touch the raceways in two points for each inner and outer contacts but not at single point for pure radial load case. Because of this, the radial play is decreased by the amount of  $(\Delta P_d)_i$  and  $(\Delta P_d)_o$  for inner and outer contacts respectively, and given in Equation 2.12.

$$P_d = S_d - (\Delta P_d)_i - (\Delta P_d)_o \quad (2.12)$$

Where;

$$(\Delta P_d)_i = (2r_i - D)(1 - \cos \alpha_{si}) \text{ and} \quad (2.13)$$

$$(\Delta P_d)_o = (2r_o - D)(1 - \cos \alpha_{so}) . \quad (2.14)$$

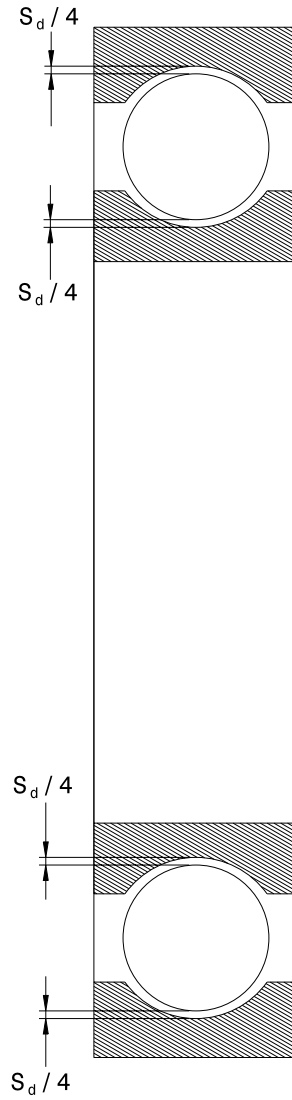


Figure 2.6: Non-arched Bearing (DGBB) Radial Clearance,  $S_d$

Finally, the unloaded contact angle,  $\alpha_0$  can be calculated via Equation 2.15.

$$\alpha_0 = \cos^{-1} \left( 1 - \frac{P_d}{2BD} \right) \quad (2.15)$$

The axial (clearance) end play of the bearing,  $P_e$  can be calculated by Equation 2.16. As seen from the equation, axial end play is also decreased by shim grinding operation. By this configuration, 4PCBBs can have higher contact angles with lower axial

end plays. However, this cannot be achieved with the conventional ACBBs.

$$P_e = 2BD \sin \alpha_0 - g_i - g_o \quad (2.16)$$

Halpin and Tran [15] visualize the internal play of 4PCBB by considering a normalized circle of radius  $2r - D$  as shown in Figure 2.7. As it is given in Figure 2.7, the relations between internal clearances, shim angles, contact angle, shim thickness and axial end-play can easily be derived from this normalized circle.

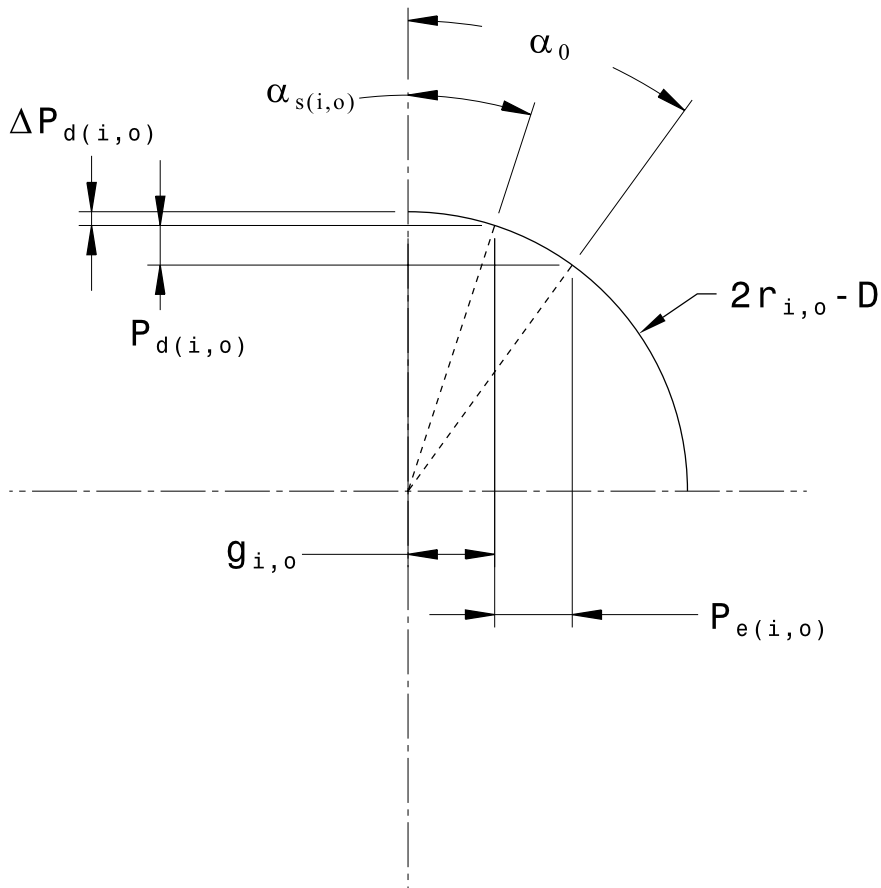


Figure 2.7: Normalized Internal Clearance Circle

The parameters that are needed for the contact stiffness calculations are described as in Section 2.1. These are basically the, curvature sum,  $\Sigma_\rho$  and curvature difference,  $F_\rho$  which are needed to be calculated for each raceway and ball contact with the loaded contact angle in order to simulate the contact stiffness in the loaded condition. Thus, the formulation for ACBBs as given in 2.1 is valid for 4PCBB.

### 2.3 Elliptical Contact Theory Application to Ball & Raceway Contacts

The Hertzian contact theory for elliptical contacts require Equation 2.17 to be solved for ellipticity parameter,  $\kappa$  for both inner and outer raceway contacts.

$$\frac{(\kappa^2 + 1) \mathcal{E}(\kappa) - 2\mathcal{F}(\kappa)}{(\kappa^2 - 1) \mathcal{E}(\kappa)} - F\rho = 0 \quad (2.17)$$

Where; terms  $\mathcal{F}$  and  $\mathcal{E}$  denote the elliptical integral of first kind and second kind, respectively. These integrals are given in Equation 2.18 & 2.19.

$$\mathcal{F}(\kappa) = \int_0^{\pi/2} \left[ 1 - \left( 1 - \frac{1}{\kappa^2} \right) \sin^2 \phi \right]^{-1/2} d\phi \quad (2.18)$$

$$\mathcal{E}(\kappa) = \int_0^{\pi/2} \left[ 1 - \left( 1 - \frac{1}{\kappa^2} \right) \sin^2 \phi \right]^{1/2} d\phi \quad (2.19)$$

In order to have an efficient model for an optimization subroutine, these contact parameters are approximated by a numerical method which is defined in Antoine's study [5]. In this study, the ellipticity parameter,  $\kappa$  is expressed by an approximate expression in the structure of Equation 2.20.

$$\kappa = (N/M)^\lambda \quad (2.20)$$

Where;

$$M = \frac{\Sigma\rho}{4}(1 - F\rho) \quad \& \quad N = \frac{\Sigma\rho}{4}(1 + F\rho). \quad (2.21)$$

Ellipticity parameter,  $\kappa$  in the form of Equation 2.20, satisfies the Equation 2.17 as in Equation 2.22

$$F\rho = \frac{N/M - 1}{N/M + 1} = \frac{(\kappa^2 + 1) \mathcal{E}(\kappa) - 2\mathcal{F}(\kappa)}{(\kappa^2 - 1) \mathcal{E}(\kappa)} \quad (2.22)$$

The exponent  $\lambda$  for describing the behaviour of  $N/M$  is approximated in the form of Equation 2.23

$$\lambda = \frac{2}{3} \left( \frac{1 + \mu_1 X^2 + \mu_2 X^4 + \mu_3 X^6 + \mu_4 X^8}{1 + \mu_5 X^2 + \mu_6 X^4 + \mu_7 X^6 + \mu_8 X^8} \right) \quad (2.23)$$

Where  $X = \log_{10}(N/M)$ , and the coefficients are tabulated in Table 2.1

Table 2.1: Coefficients for Exponent,  $\lambda$  [5]

$\mu_1$	0.40227436	$\mu_5$	0.42678878
$\mu_2$	$3.7491752 \times 10^{-2}$	$\mu_6$	$4.2605401 \times 10^{-2}$
$\mu_3$	$7.4855761 \times 10^{-4}$	$\mu_7$	$9.0786922 \times 10^{-4}$
$\mu_4$	$2.1667028 \times 10^{-6}$	$\mu_8$	$2.7868927 \times 10^{-6}$

The elliptical integrals are also approximated as in Equation 2.24 & Equation 2.25

$$\mathcal{F}(\kappa) = (\zeta_0 + \zeta_1 m_1 + \zeta_2 m_1^2) - (\zeta_3 + \zeta_4 m_1 + \zeta_5 m_1^2) \ln m_1 \quad (2.24)$$

$$\mathcal{E}(\kappa) = (\beta_0 + \beta_1 m_1 + \beta_2 m_1^2) - (\beta_3 m_1 + \beta_4 m_1^2) \ln m_1 \quad (2.25)$$

Where  $m_1 = 1/\kappa^2$  and the coefficients are tabulated in Table 2.2.

Table 2.2: Coefficients for Approximated Polynomials of Elliptical Integrals [5]

$\zeta_0$	1.3862944	$\beta_0$	1
$\zeta_1$	0.1119723	$\beta_1$	0.4630151
$\zeta_2$	0.0725296	$\beta_2$	0.1077812
$\zeta_3$	0.5	$\beta_3$	0.2452727
$\zeta_4$	0.1213478	$\beta_4$	0.0412496
$\zeta_5$	0.0288729		

By the help of the approximation functions given in [5], which are explained above, the corresponding ellipticity parameter,  $\kappa$ , and the elliptical integral of first kind and second kind,  $\mathcal{F}(\kappa)$ ,  $\mathcal{E}(\kappa)$  are obtained. By the help of this parameters and the

elliptical integrals, the load-deflection relationship, ( $Q$  vs.  $\delta$ ) can be established with the following formulae:

$$Q = K\delta^{3/2} \quad (2.26)$$

$$Q = \left[ \frac{2^{(5/2)}}{3} \frac{E^*}{(\delta^*)^{3/2} [(M + N)/2]^{1/2}} \right] \delta^{3/2} \quad (2.27)$$

Where  $E^*$  is the equivalent modulus of elasticity, which is derived from the materials' properties  $[E_I, \nu_I]$  and  $[E_{II}, \nu_{II}]$  for bodies I and II respectively. This relation is given in Equation 2.28. Equivalent modulus of elasticity,  $E^*$  for both inner raceway and outer raceway contacts are equal since both raceways; inner and outer are assumed to have the same material properties.

$$\frac{1}{E^*} = \frac{1 - \nu_I^2}{E_I} + \frac{1 - \nu_{II}^2}{E_{II}} \quad (2.28)$$

Dimensionless parameters,  $a^*$ ,  $b^*$  and  $\delta^*$  that are required for defining the contact ellipse dimensions and the contact deflection are given in Equation 2.29, 2.30 and 2.31, respectively.

$$a^* = \left[ \frac{2\kappa^2 \mathcal{E}(\kappa)}{\pi} \right]^{1/3} \quad (2.29)$$

$$b^* = \left[ \frac{2\mathcal{E}(\kappa)}{\pi\kappa} \right]^{1/3} \quad (2.30)$$

$$\delta^* = \frac{2\mathcal{F}(\kappa)}{\pi} \left[ \frac{\pi}{2\kappa^2 \mathcal{E}(\kappa)} \right]^{1/3} \quad (2.31)$$

Dimensions of contact ellipse,  $a$ ,  $b$  and mutual approach of the centers of both bodies,  $\delta$  are given by following formulae:

$$a = a^* \left[ \frac{3Q}{4(M+N)E^*} \right]^{1/3} \quad (2.32)$$

$$b = b^* \left[ \frac{3Q}{4(M+N)E^*} \right]^{1/3} \quad (2.33)$$

$$\delta = \delta^* \left[ \frac{3Q}{2E^*} \right]^{2/3} \frac{[(M+N)/2]^{1/3}}{2} \quad (2.34)$$

The maximal contact stress occurring on the contact ellipse,  $\sigma$  is obtained with Equation 2.35

$$\sigma = \frac{3}{2} \frac{Q}{\pi ab} \quad (2.35)$$

To conclude, in this approximation method, the Hertzian theory results show that the errors are within the  $\pm 30$  ppm range [5] (Error unit: part per million,  $1 \text{ ppm} = 10^{-4} \%$ ). This accuracy is sufficient for the calculation of the contact stiffness,  $K$ . The procedure given in this section is aimed to find the contact stiffness with the given bearing geometry and material properties. This procedure shall be applied on each rolling element and each raceway contacts within the bearing.

## CHAPTER 3

### MATHEMATICAL MODEL FOR THE LOAD DISTRIBUTION OF 4PCBB

In rolling contact bearings, the utility of the load distribution models is to provide the correlation between the applied ring loads and the ring deflections. For this purpose, the rolling element loads which resulted in raceway contacts need to be found in a quasi-static condition.

In this Chapter, the models existing in the literature are examined, united and modified in order to obtain a robust and an efficient model for optimization algorithm.

First of all, the coordinate system that referenced through the study is introduced in Figure 3.1. As seen from the figure, the direction  $Z$  is the axial direction for the bearing. The other axis  $X$  and  $Y$  are utilized for the radial directions.

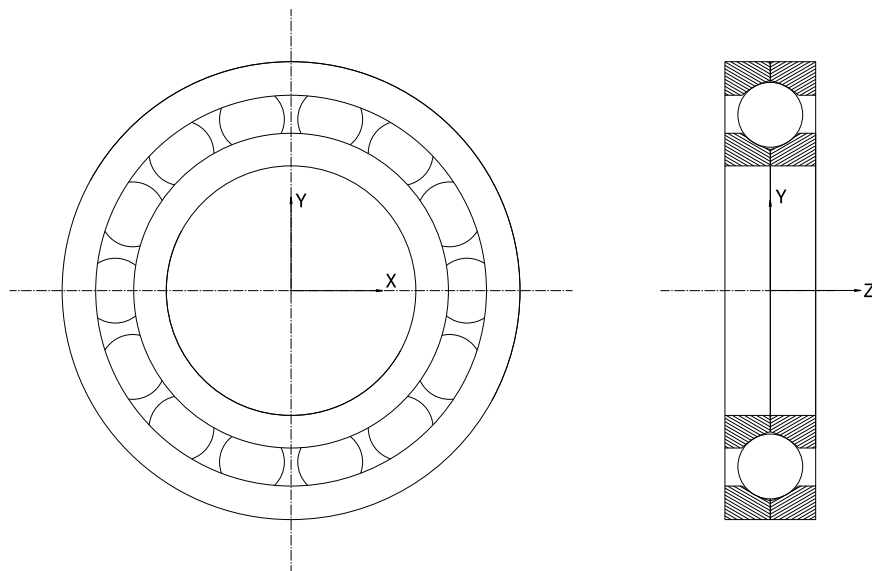


Figure 3.1: Coordinate System of the Bearing

The first rolling element is placed on the X axis. The other rolling elements are numbered with respect to Figure 3.2. Moreover, azimuth angles,  $\Psi_j$  of these rolling elements are also illustrated in Figure 3.2. The total number of balls within the bearing is symbolized by  $Z$ , and the azimuth angles for each ball,  $\Psi_j$  is formulated in Equation 3.1 where subscript  $j$  stands for ball number such as:  $j = 1, 2, \dots, Z$ .

$$\Psi_j = (j - 1) \frac{2\pi}{Z} \quad (3.1)$$

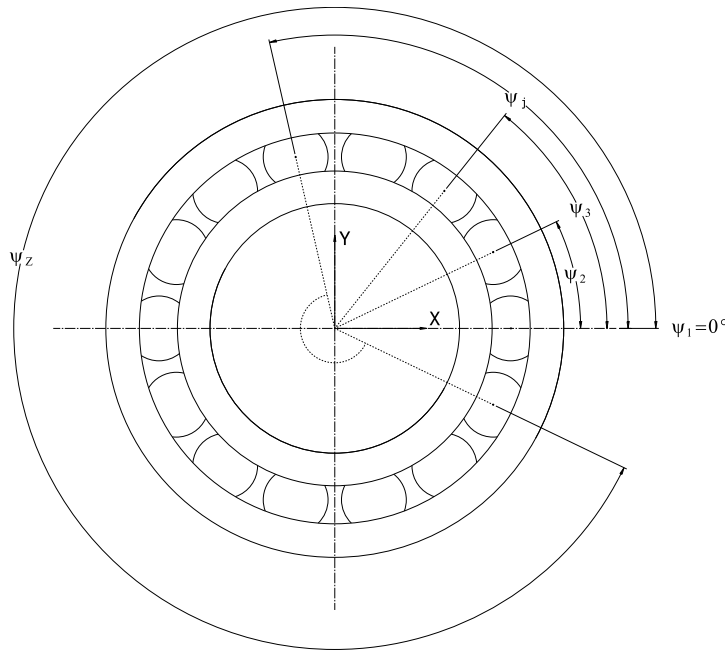


Figure 3.2: Ball Numbering and Azimuth Angles

### 3.1 Comparison with Conventional Ball Bearing Load Distribution Models

It carries great importance to inspect the ball bearing load distribution models for good understanding of the geometrical parameters and their role within a ball bearing. Therefore, for this study, ball bearing load distribution models of conventional bearings have been investigated. Load distribution models of conventional DGBBs and ACBBs without centrifugal effects were the essential step to overcome in order to be familiar with ball bearing theory. In ISO16281 [4], the basic concepts for generating a load distribution model for ball bearings are summarized. In the model given in

ISO16281 [4], there exist single sets of loaded contact angles,  $\alpha_j$  for both inner and outer raceway contacts. Moreover, the contact stiffness for inner and outer contacts are serially summed up as in Equation 3.2. Therefore, contact deflection,  $\delta_j$  is the sum of inner and outer contact deflections which are assumed to be equal. Thus, for a quasi-static ball there exist  $2 \times Z$  unknowns to be solved which are  $\alpha_j$  and  $\delta_j$ .

$$\frac{1}{K_{io}} = \frac{1}{K_i} + \frac{1}{K_o} \quad (3.2)$$

Once the centrifugal effects are included in the model, the kinematics of the bearing become more complicated. The contact load between ball and outer ring,  $Q_{oj}$  increases because of the centrifugal loads,  $F_{cj}$  acting on balls towards to outer ring direction. Furthermore, this makes contact angles for inner and outer contacts to be different i.e. the outer loaded contact angle,  $\alpha_{oj}$  decreases. For this case, there exist  $4 \times Z$  unknowns which are  $\delta_{ij}$ ,  $\delta_{oj}$ ,  $\alpha_{ij}$  and  $\alpha_{oj}$  to be solved for quasi-static ball. These kinematic differences are illustrated in Figure 3.3 for the conventional ball bearing without and with centrifugal effects.

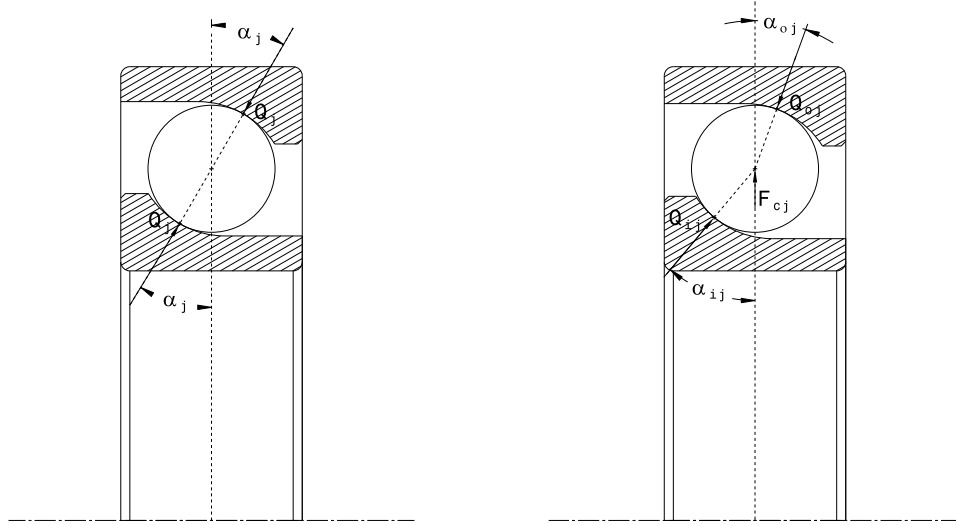


Figure 3.3: Ball Equilibrium in a Conventional Ball Bearing with Centrifugal Effects  
i. Not included ii. Included

Kinematics of the 4PCBBs becomes much more complicated by the employment of unique geometrical parameters and the nature of the possible contacts on four different points. Namely, there exist unknowns in the number of  $8 \times Z$  that needed to

be solved within the mathematical model for the load distribution of a 4PCBB.

### 3.2 General Structure of the Mathematical Model of 4PCBB

In this section, overview of the generated model is briefly explained in terms of the inputs & outputs. Moreover, the flowchart of the established model is provided at the Appendix A.4.

The input parameters are divided into three categories as shown in the flowchart. These categories are geometry, loading and material inputs. Geometry inputs consist the 4PCBB geometrical parameters which defines the bearing geometry. The parameters  $S_d, g_i, g_o$  are sufficient for calculating the free (unloaded) contact angle,  $\alpha_0$ . Therefore, the unloaded contact angle is not given as an input but a calculated parameter before the iterations.

The loading inputs are simply the applied ring load matrix  $F$  and the rotational speed,  $\omega$ . The load matrix,  $F$  consist the 5 DoF loading such as;

$$F = \begin{bmatrix} F_x \\ F_y \\ F_z \\ M_x \\ M_y \end{bmatrix} \quad (3.3)$$

This loading and the speed produce a corresponding ring displacement matrix,  $\delta$  such as;

$$\delta = \begin{bmatrix} \delta_x \\ \delta_y \\ \delta_z \\ \beta_x \\ \beta_y \end{bmatrix} \quad (3.4)$$

Since the outer ring is assumed to be fixed, and the load is applied to the inner ring, the load matrix and the ring displacements are assumed to occur at the inner ring. These load and displacement matrices are located and oriented as in the coordinate

system given in Figure 3.1.  $F_x, F_y, F_z$  are the applied ring loads in X, Y and Z directions, respectively.  $M_x$  and  $M_y$  are the applied ring moments in X and Y directions. For the displacements,  $\delta_x, \delta_y, \delta_z$  are the ring displacements in X, Y and Z directions, respectively.  $\beta_x, \beta_y$  are the rotational displacements along X and Y directions, respectively. The other parameter is the rotational speed,  $\omega$  which is an important parameter for centrifugal effect calculations. For this study, it is assumed that the inner ring is rotating and outer ring is stationary. However, there exist methods in the literature to establish centrifugal effects for other cases. [6]

The last category of the inputs for the model is the material. The elastic modulus of the bodies,  $E_{i,o,b}$  (inner & outer rings and the balls) as well as the poisson's ratio  $\nu_{i,o,b}$  are required for contact stiffness calculations. For the centrifugal effects, the density of the balls,  $\rho_b$  is another needed parameter.

After the pre-calculations are carried out, iterations are started with initial guesses in order to solve the necessary constraint equations which define the bearing quasi-static condition for a load and speed case. After iterations converge to a solution the loaded internal geometry and internal load distribution of the bearing is obtained for a given load and speed case. After obtaining these results, by the help of post-process calculations, the contact stresses of each contact over each rolling element can be found.

### 3.3 Kinematics of the Quasi-Static Ball of 4PCBB

In this Section, the kinematics of the ball equilibrium is investigated. The relations between the inner ring displacements,  $(\delta_x, \delta_y, \delta_z, \beta_x, \beta_y)$  and the contact deformations  $(\delta_{il}, \delta_{ir}, \delta_{ol}, \delta_{or})$  as well as the contact angles  $(\alpha_{il}, \alpha_{ir}, \alpha_{ol}, \alpha_{or})$  are established. For this purpose, ball and raceway centers at initial and at deformed conditions are illustrated as in Figure 3.4. In Figure 3.4,  $C_{mk}$ 's are the raceway centers where subscript  $m = i, o$  for inner or outer, and subscript  $k = l, r$  for left or right respectively. As shown in Figure 3.4, since the outer ring in the bearing is assumed to be fixed,  $C_{ol}$  and  $C_{or}$  are at the same position at initial and at deformed state. On the other hand, the inner raceway centers for left and right ( $C_{il}$  and  $C_{ir}$ ) take the position  $C'_{il}$  and

$C'_{ir}$  after the displacements and deformations within the bearing. Similarly, ball center moves to the deformed position  $O'$  from the initial position  $O$ . By this way, the shown contact angles,  $\alpha_{il}$ ,  $\alpha_{ir}$ ,  $\alpha_{ol}$ ,  $\alpha_{or}$  are formed. Distances between the left and right raceways for both inner and outer raceways, shall be  $g_i$  and  $g_o$ , respectively.

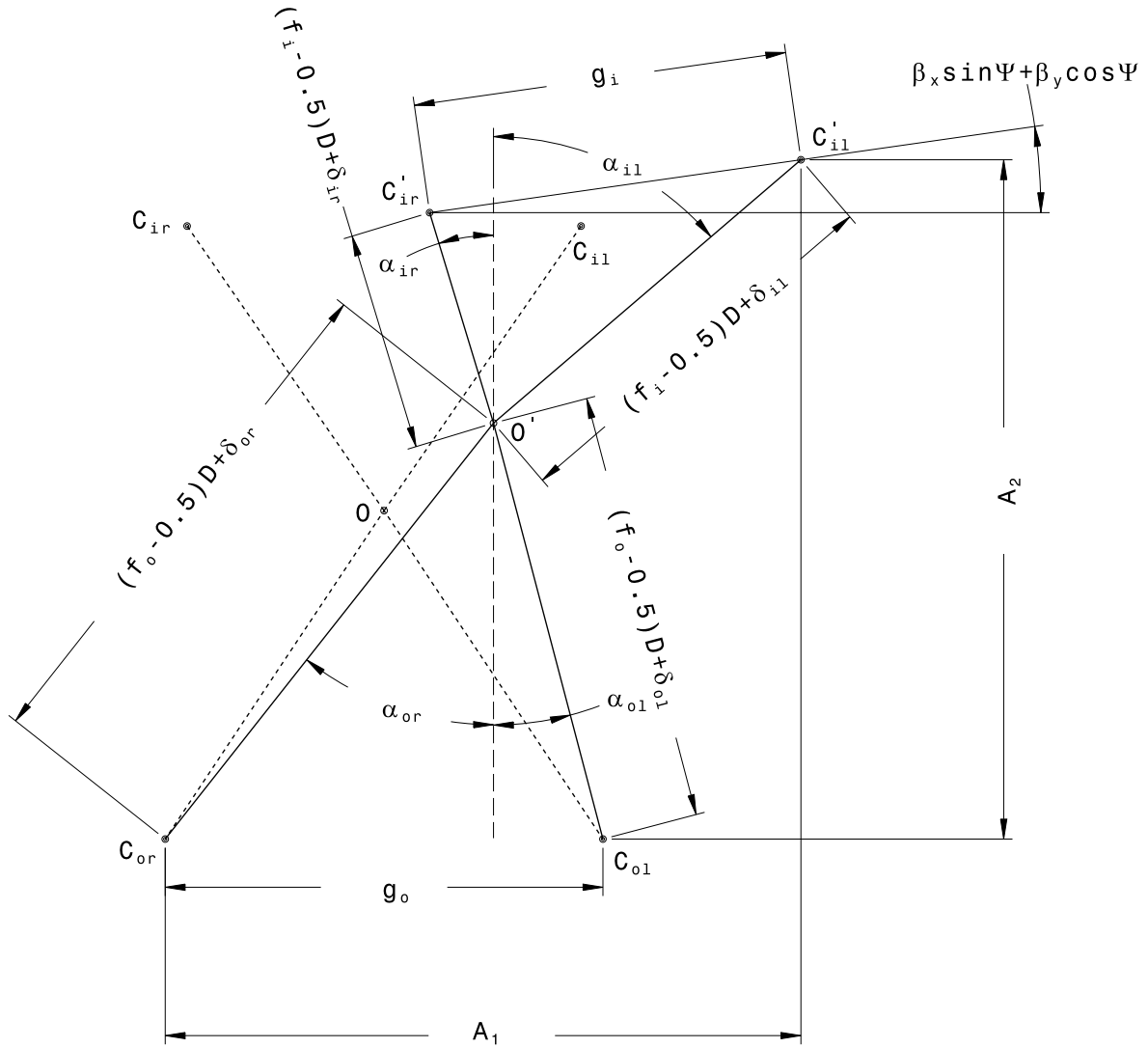


Figure 3.4: Ball and Raceway Centers at Initial and Deformed Positions

Auxiliary parameters  $A_1$  and  $A_2$  are the resultant of the ring displacements,  $\delta_x$ ,  $\delta_y$ ,  $\delta_z$ ,

$\beta_x, \beta_y$  and stated as in Equation 3.5 and 3.6.

$$A_{1,j} = BD \sin \alpha_0 + \delta_z - R_i(\beta_x \sin \Psi_j + \beta_y \sin \Psi_j) \quad (3.5)$$

$$A_{2,j} = BD \cos \alpha_0 + \delta_x \cos \Psi_j + \delta_y \sin \Psi_j + R_i \left[ \frac{\beta_x^2}{2} \sin \Psi_j \text{SGN}(\beta_x) + \frac{\beta_y^2}{2} \cos \Psi_j \text{SGN}(\beta_y) \right] \quad (3.6)$$

Where  $R_i$  is the distance from bearing rotation axis to inner raceway curvature center and formulated as in Equation 3.7.

$$R_i = \frac{d_m}{2} + \left( r_i - \frac{D}{2} \right) \cos \alpha_0 \quad (3.7)$$

As seen from Figure 3.4, there are several constraints for the raceway centers and the internal kinematic parameters must obey in this configuration. These constraint equations for each rolling element,  $j$  are formulated as in Equations 3.8 to 3.13. These equations are obtained from the kinematic loops given in Figure 3.4.

$$CT_{i1,j} \Rightarrow 0 = ((f_o - 0.5)D + \delta_{ol,j}) \cos \alpha_{ol,j} - ((f_o - 0.5)D + \delta_{or,j}) \cos \alpha_{or,j} \quad (3.8)$$

$$CT_{i2,j} \Rightarrow 0 = ((f_o - 0.5)D + \delta_{ol,j}) \sin \alpha_{ol,j} + ((f_o - 0.5)D + \delta_{or,j}) \sin \alpha_{or,j} - g_o \quad (3.9)$$

$$CT_{i3,j} \Rightarrow 0 = ((f_i - 0.5)D + \delta_{il,j}) \cos \alpha_{il,j} - ((f_i - 0.5)D + \delta_{ir,j}) \cos \alpha_{ir,j} - g_i \sin (\beta_x \sin \Psi_j + \beta_y \cos \Psi_j) \quad (3.10)$$

$$CT_{i4,j} \Rightarrow 0 = ((f_i - 0.5)D + \delta_{il,j}) \sin \alpha_{il,j} + ((f_i - 0.5)D + \delta_{ir,j}) \sin \alpha_{ir,j} - g_i \cos (\beta_x \sin \Psi_j + \beta_y \cos \Psi_j) \quad (3.11)$$

$$CT_{i5,j} \Rightarrow 0 = ((f_o - 0.5)D + \delta_{or,j}) \sin \alpha_{or,j} + ((f_i - 0.5)D + \delta_{il,j}) \sin \alpha_{il,j} - A_{1,j} \quad (3.12)$$

$$CT_{i6,j} \Rightarrow 0 = ((f_o - 0.5)D + \delta_{or,j}) \cos \alpha_{or,j} + ((f_i - 0.5)D + \delta_{il,j}) \cos \alpha_{il,j} - A_{2,j} \quad (3.13)$$

The constraints  $CT_{1..6}$  are established with the above formulation. As seen from Equations 3.8 to 3.13, these constraints are required to be assured for all rolling

elements i.e  $j = 1 \dots Z$ . In other words, above constraints are need to be applied for total number of balls which results a total number of  $6 \times Z$  equations to be satisfied.

### 3.4 Ball Equilibrium of 4PCBB under Contact & Body Forces

In Section 3.3, the kinematic constraints are built. In the internal loop, given in the flowchart in Appendix A, there exist  $8 \times Z$  unknowns which are the contact angles,  $\alpha_{il}, \alpha_{ir}, \alpha_{ol}, \alpha_{or}$  and the contact deflections,  $\delta_{il}, \delta_{ir}, \delta_{ol}, \delta_{or}$ , to be solved iteratively. Therefore, there remain  $2 \times Z$  equations to be established for solving these parameters. These equations are derived from the free body diagram of the rolling elements for an equilibrium condition which is given in Figure 3.5.

In order to establish equilibrium equations for the balls, it is needed to find the contact stiffness of each ball for each contact. The formulation given in Section 2.3 is used by employing the contact angles  $\alpha_{il,j}, \alpha_{ir,j}, \alpha_{ol,j}, \alpha_{or,j}$  in order to find the corresponding curvature sum,  $\Sigma\rho$  and curvature difference,  $F(\rho)$  by inputting contact angles in  $\gamma$  formulation as in Equation 2.9. Finally, the contact stiffnesses,  $K_{il,j}, K_{ir,j}, K_{ol,j}, K_{or,j}$  are found. These contact stiffnesses are utilized for contact load calculations as in Equations 3.14 to 3.17.

$$Q_{il,j} = K_{il,j} \max(0, \delta_{il,j})^{1.5} \quad (3.14)$$

$$Q_{ir,j} = K_{ir,j} \max(0, \delta_{ir,j})^{1.5} \quad (3.15)$$

$$Q_{ol,j} = K_{ol,j} \max(0, \delta_{ol,j})^{1.5} \quad (3.16)$$

$$Q_{or,j} = K_{or,j} \max(0, \delta_{or,j})^{1.5} \quad (3.17)$$

In Equations 3.14 to 3.17 the contact deflections,  $\delta_{mk,j}$  shall be taken as zero in case of negative deflections which means no contact occurs in that specific ball and specific contact.

After finding the contact loads,  $Q_{mk,j}$ , the remaining constraints  $CT_{7,j}$  and  $CT_{8,j}$  are formulated in Equations 3.18 and 3.19 with respect to Figure 3.5.

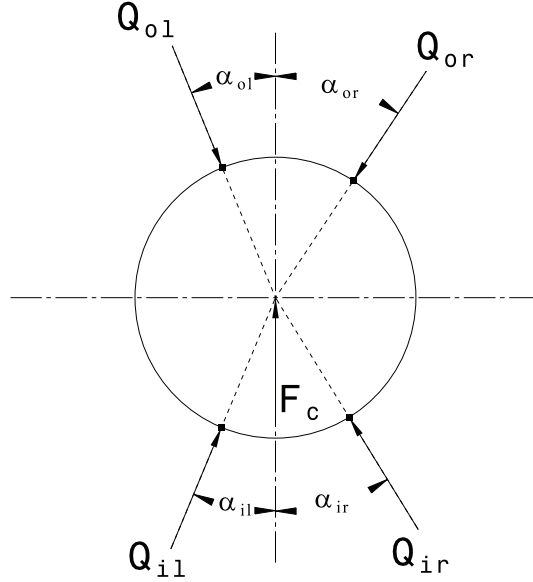


Figure 3.5: Ball at Equilibrium Condition

$$CT_{i7,j} \Rightarrow 0 = Q_{il,j} \sin \alpha_{il,j} + Q_{ol,j} \sin \alpha_{ol,j} - Q_{ir,j} \sin \alpha_{ir,j} - Q_{or} \sin \alpha_{or} \quad (3.18)$$

$$CT_{i8,j} \Rightarrow 0 = Q_{il,j} \cos \alpha_{il,j} + Q_{ir,j} \cos \alpha_{ir,j} - Q_{ol,j} \cos \alpha_{ol,j} - Q_{or} \cos \alpha_{or} + F_{c,j} \quad (3.19)$$

Where  $F_{c,j}$  is the centrifugal forces acting on the rolling elements. The formulation of the centrifugal force is given as in Equation 3.20.

$$F_{c,j} = \rho_b \frac{4\pi \left(\frac{D}{2}\right)^3}{3} \frac{d_m}{2} \Omega^2 \quad (3.20)$$

Where  $\rho_b$  is the density of the balls, and the  $\Omega$  is the ball orbital speed or separator (cage) speed. For the calculation of the orbital speed,  $\Omega$ , several assumptions are made for an efficient model. In this study, it is aimed to make an optimization for a 4PCBB to act like an ACBB. Although Halpin [15] proposes that the Jones' [6] "race

control theory" becomes untenable for frictional effects calculation for a 4PCBB with possible four point contacts, Jones' theory is applied for this study. Since the frictional and gyroscopic moment effects are disregarded in this study, Jones' model is still applicable for calculation of body forces which results from centrifugal effects.

Raceway control theory assumes that the ball rolls on one raceway without spinning and all the spin occurs with respect to the other raceway. The raceway which the rolling occurs called as the "controlled raceway".

The orbital speed,  $\Omega$  formulation is given in Equation 3.21 for inner ring rotating and outer raceway controlled bearing. The other cases are also given in detail in Jones' study [6].

$$\Omega_j = \omega \frac{1 - \gamma' \cos \alpha_{ik,j}}{1 + \cos (\alpha_{ik,j} - \alpha_{ok,j})} \quad (3.21)$$

Where  $\gamma'$  is the ratio of ball diameter to pitch diameter such as:  $\gamma' = D/dm$ . As proposed in [15], for the contact angles,  $\alpha_{ik,j}$  and  $\alpha_{ok,j}$ , the raceways are selected for subscript  $k$  upon which raceway provide the dominating tractive forces. It can be guaranteed to obey this rule by making an analogy with the direction of axial load,  $F_z$  and the dominating raceways. This analogy is given in Equation 3.22.

$$k = \begin{cases} l, & \text{if } m = i \text{ and } F_z > 0 \\ r, & \text{if } m = o \text{ and } F_z > 0 \\ r, & \text{if } m = i \text{ and } F_z < 0 \\ l, & \text{if } m = o \text{ and } F_z < 0 \end{cases} \quad (3.22)$$

As an example, for an applied axial load,  $F_z$  in +Z direction, the dominating raceways will be inner left, ( $m = i, k = l$ ) and outer right raceway, ( $m = o, k = r$ ).

### 3.5 Bearing Reaction Force vs. Applied Ring Load

In Sections 3.3 and 3.4, the constraints that need to be satisfied within the internal loop is provided. In this Section, the outer loop constraints are established with equating

the bearing reaction forces to the applied loads. Once the internal loop constraints are satisfied with a pre-assumed ring displacements,  $\delta$  in outer loop, the internal loop variables ( $\delta_{mk,j}$  and  $\alpha_{mk,j}$ ) are solved iteratively within the generated mathematical model. After that, resultant internal loop variables are supplied to the outer loop. In the outer loop, the iterating independent variables are the ring displacements,  $\delta$  for finding the overall resulting bearing reaction matrix,  $(F)_{reaction}$  which is given as in Equation 3.23.

$$(F)_{reaction} = \begin{bmatrix} (F_x)_{reaction} \\ (F_y)_{reaction} \\ (F_z)_{reaction} \\ (M_x)_{reaction} \\ (M_y)_{reaction} \end{bmatrix} \quad (3.23)$$

The outer loop constraints are established by  $(F)_{reaction} - F = 0$ . These constraints,  $CT_{o1}$  to  $CT_{o5}$  are given in Equations 3.24 to 3.28, respectively.

$$CT_{o1} \Rightarrow 0 = \left[ \sum_{j=1}^Z (Q_{il,j} \cos \alpha_{il,j} + Q_{ir,j} \cos \alpha_{ir,j}) \cos \Psi_j \right] - F_x \quad (3.24)$$

$$CT_{o2} \Rightarrow 0 = \left[ \sum_{j=1}^Z (Q_{il,j} \cos \alpha_{il,j} + Q_{ir,j} \cos \alpha_{ir,j}) \sin \Psi_j \right] - F_y \quad (3.25)$$

$$CT_{o3} \Rightarrow 0 = \left[ \sum_{j=1}^Z (Q_{il,j} \sin \alpha_{il,j} + Q_{ir,j} \sin \alpha_{ir,j}) \right] - F_z \quad (3.26)$$

$$CT_{o4} \Rightarrow 0 = \left[ \sum_{j=1}^Z R_i (Q_{il,j} \sin \alpha_{il,j} - Q_{ir,j} \sin \alpha_{ir,j}) \sin \Psi_j \right] - M_x \quad (3.27)$$

$$CT_{o5} \Rightarrow 0 = \left[ \sum_{j=1}^Z -R_i (Q_{il,j} \sin \alpha_{il,j} - Q_{ir,j} \sin \alpha_{ir,j}) \cos \Psi_j \right] - M_y \quad (3.28)$$

Finally, after both internal and outer loop iterations are converged to a solution, the corresponding independent iterating variables are found. Namely, the internal load distribution,  $Q_{mk,j}$ , contact angles,  $\alpha_{mk,j}$ , contact deflections,  $\delta_{mk,j}$  as well as the ring displacement matrix,  $\delta$  are the output of the mathematical model. By the help of these results, it is possible to calculate the necessary parameters such as: contact

stress, ellipse truncation etc. for the evaluation of the bearing performance.

### 3.6 Postprocess for Ellipse Truncation Calculations

In order to evaluate the bearing performance and behaviour under a specific operating condition, it is necessary to investigate the several phenomena. In bearing literature, one of the most important performance parameter is the bearing life. Significant numbers of studies are made on bearing life calculations. To illustrate, in ISO 281 [18], the bearing dynamic load rating and rating life calculations are presented. However, in this standard, only axial and radial loadings are taken into account, and combined for finding the equivalent load. In this method, the bearing internal load distribution is not taken into account. In ISO 16281 [4], the moment loadings are included, as well as the load distribution effects on bearing life. However, in this standard, the centrifugal effects are not included in the calculations.

Besides, the bearing life is very much dependent on the operating conditions such as: lubrication, contamination and bearing material. These factors are needed to be included for a reliable estimation of the bearing life. Therefore, in this study, it is aimed to evaluate the bearing performance over the resulting contact stresses and possible ellipse truncations. The contact stress calculations are given in Section 2.3. Therefore, the other phenomenon; "Ellipse Truncation" and the calculation method is explained in this section.

In ball bearings, ellipse truncation is defined as the incidence of the ball and raceway contact zones to exceed the edge of the raceway as given in Figure 3.6. Upon this incidence occurs, the stress at the edge of the contact increases rapidly with the fraction truncated, and the stress at the center of the contact also increases as the total area of the contact is decreased. Therefore, the bearing materials yield at a lower applied load than without truncation. Therefore, for performance evaluation of a bearing, it carries great importance to control the ellipse truncation.

After obtaining the loaded contact angles and contact ellipse shape, geometrical calculations are needed to find out the situation in terms of the ellipse truncation as in Figure 3.7. Firstly, the shoulder diameters,  $D_{sk}$ , which are assumed to be equal for

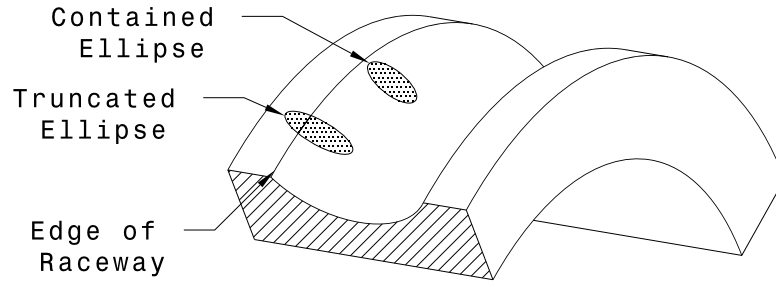


Figure 3.6: Ellipse Truncation

left and right raceways, need to be given for inner and outer raceway. For this purpose, shoulder thicknesses,  $St_i$  are employed in the form of a multiplication with ball diameter in order to have a good sense in relating to ball diameter. To illustrate, usually shoulder thickness is in between 0.15 to 0.30 times the ball diameter ( $St_i = 0.15D$  to  $0.30D$ ). Thus, shoulder diameters,  $D_{sk}$  are found with Equations 3.29 and 3.30;

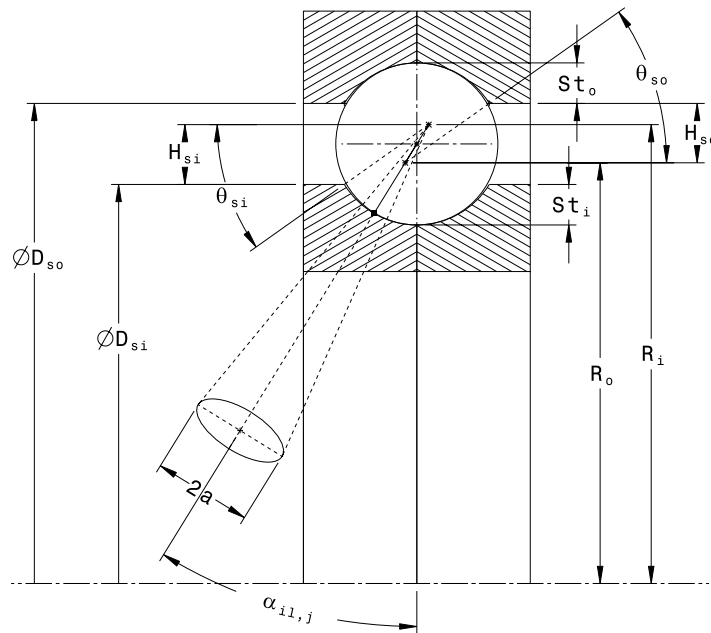


Figure 3.7: Contact ellipse at the loaded contact angle

$$D_{si} = d_m - D + 2St_i \quad (3.29)$$

$$D_{so} = d_m + D - 2St_i \quad (3.30)$$

Furthermore, the vertical distance between the shoulder diameter and raceway curvatures,  $H_{sk}$  are found as in Equations 3.31 and 3.32.

$$H_{si} = R_i - \frac{D_{si}}{2} \quad (3.31)$$

$$H_{so} = \frac{D_{so}}{2} - R_o \quad (3.32)$$

The shoulder edge angles,  $\theta_{sk}$  are needed to be formulated in order to obtain the limits of the edge, and given for inner and outer shoulders in Equations 3.33 and 3.34, respectively.

$$\theta_{si} = \sin^{-1} \frac{H_{si}}{r_i} \quad (3.33)$$

$$\theta_{so} = \sin^{-1} \frac{H_{so}}{r_o} \quad (3.34)$$

The truncation quantity is usually given in the form of percentage of semi-major axis of the contact ellipse,  $a_{km,j}$  in order to indicate the portion of the ellipse that exceeds the shoulder edge. Thus, the truncation in percentage for each rolling element and for each inner and outer raceway contacts,  $TR_{k,j}$  is given in Equation 3.35.

$$TR_{k,j} = 100 \frac{\left[ \alpha_{km,j} + \sin^{-1} \left( \frac{a_{km,j}}{r_k} \right) \right] - [\pi/2 - \theta_{sk}]}{2 \sin^{-1} \left( \frac{a_{km,j}}{r_k} \right)} \quad (3.35)$$

If the output of the above formulation is negative, then it indicates that there exists no ellipse truncation, and all the semi-major axis of the contact is contained within the raceway.

### 3.7 Results of the Load Distribution Mathematical Model

In this section, the mathematical model results are given for a bearing under different loading conditions. These loads are selected for simulating axial dominant load,

radial dominant load and moment induced loads with A, B and C respectively. These loading conditions are given in Table 3.1.

Table 3.1: Loads for the Results

	Load A	Load B	Load C
$F_x$ [N]	1500	-5000	1000
$F_y$ [N]	0	2500	1500
$F_z$ [N]	5000	1000	3000
$M_x$ [Nm]	0	0	65
$M_y$ [Nm]	0	0	-40
$n$ [rpm]	23000	23000	23000

The bearing design including the geometrical inputs as well as the pre-calculated geometrical parameters are given in Table 3.2. The material properties are selected same for both raceways and balls. ( $E_{i,o,b} = 208000$  MPa,  $\nu_{i,o,b} = 0.3$ ,  $\rho_b = 7850$  kg/m<sup>3</sup>)

Table 3.2: Geometrical Parameters of the Bearing

Geometrical Inputs			Pre-calculated Parameters		
	Value	Unit		Value	Unit
			$r_i$	5.335	mm
$d_m$	72.480	mm	$r_o$	5.376	mm
$D$	10.319	mm	$\alpha_{si}$	15.710	$^\circ$
$Z$	16	#	$\alpha_{so}$	12.662	$^\circ$
$f_i$	0.517	-	$\Delta P_{di}$	0.013	mm
$f_o$	0.521	-	$\Delta P_{do}$	0.011	mm
$g_i$	0.095	mm	$P_d$	0.063	mm
$g_o$	0.095	mm	$\alpha_0$	23.188	$^\circ$
$S_d$	0.087	mm	$P_e$	0.119	mm
$St/D$	0.300	-	$R_i$	36.401	mm
			$R_o$	36.041	mm

For the Load A, as seen from Figure 3.8, with the dominating axial load, the bearing acts like an ACBB in the operation which is a desirable case. The two raceways, inner-left and outer-right are loaded by making contacts with the balls. However,

the other two raceways, inner-right and outer-left, have no contact loads. Moreover, because of the centrifugal load, outer contact loads are higher than the inner ones. In addition, loaded contact angles in outer raceway are lower than the inner raceway. Although, the outer contact loads are higher than the inner ones, the maximum contact stresses in outer contacts are lower than the inner ones. The reason of this situation is because of the curvature sum and difference as well as the osculation parameters of the inner and outer raceways.

For the Load B, the four point contact is observed in the bearing rolling elements because of the dominant radial load. This makes the bearing to operate in an undesirable condition with the high risk of excess heat generation because of sliding. Therefore, the transition from two point contact to possible three or four point contact shall be captured and bearing shall be suitably designed and optimized in order to operate like in the Load A. If this is not possible for a specific application then it is beneficial to switch to a design with two rows of bearing.

The combined moment loading is also another reason for a 4PCBB to have three or four point contact in the balls as seen in Figure 3.10. Since moment loading makes the inner ring to be tilted, the opposite raceways are loaded within the bearing for ball numbers separated by azimuth angle of  $180^\circ$ . Therefore, by this opposite loading, the four point contact within the bearing becomes probable.

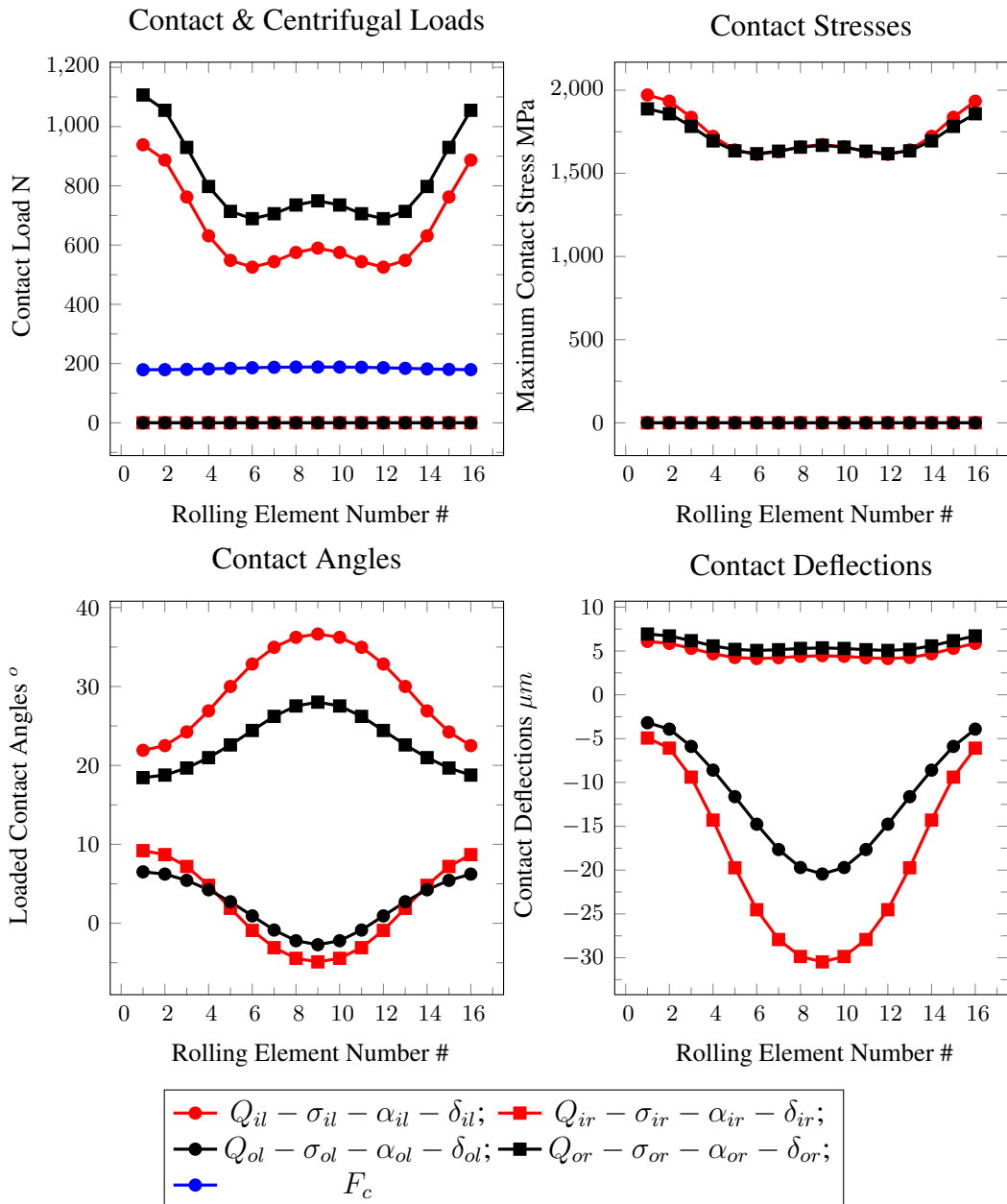


Figure 3.8: Results for Load A

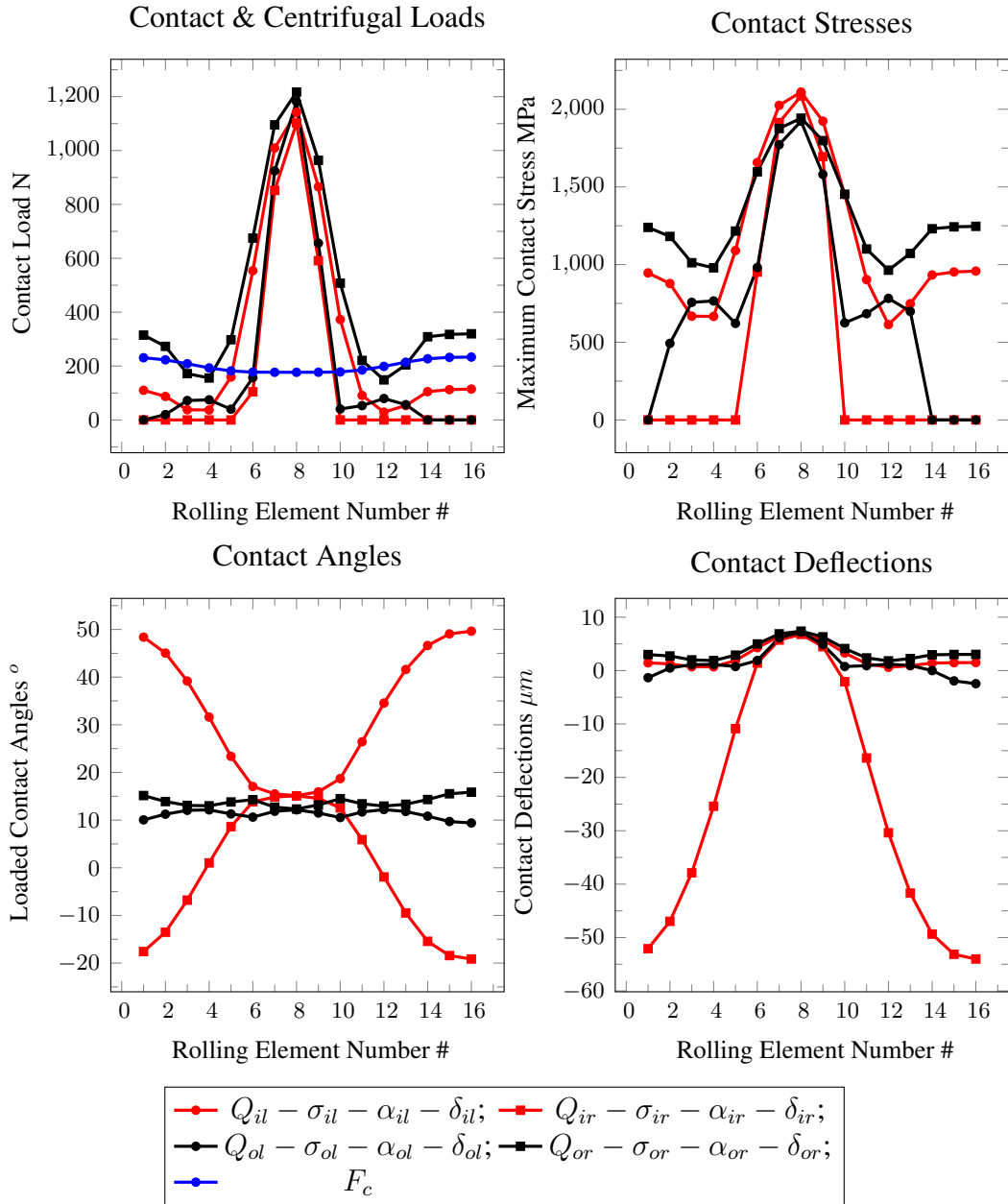


Figure 3.9: Results for Load B

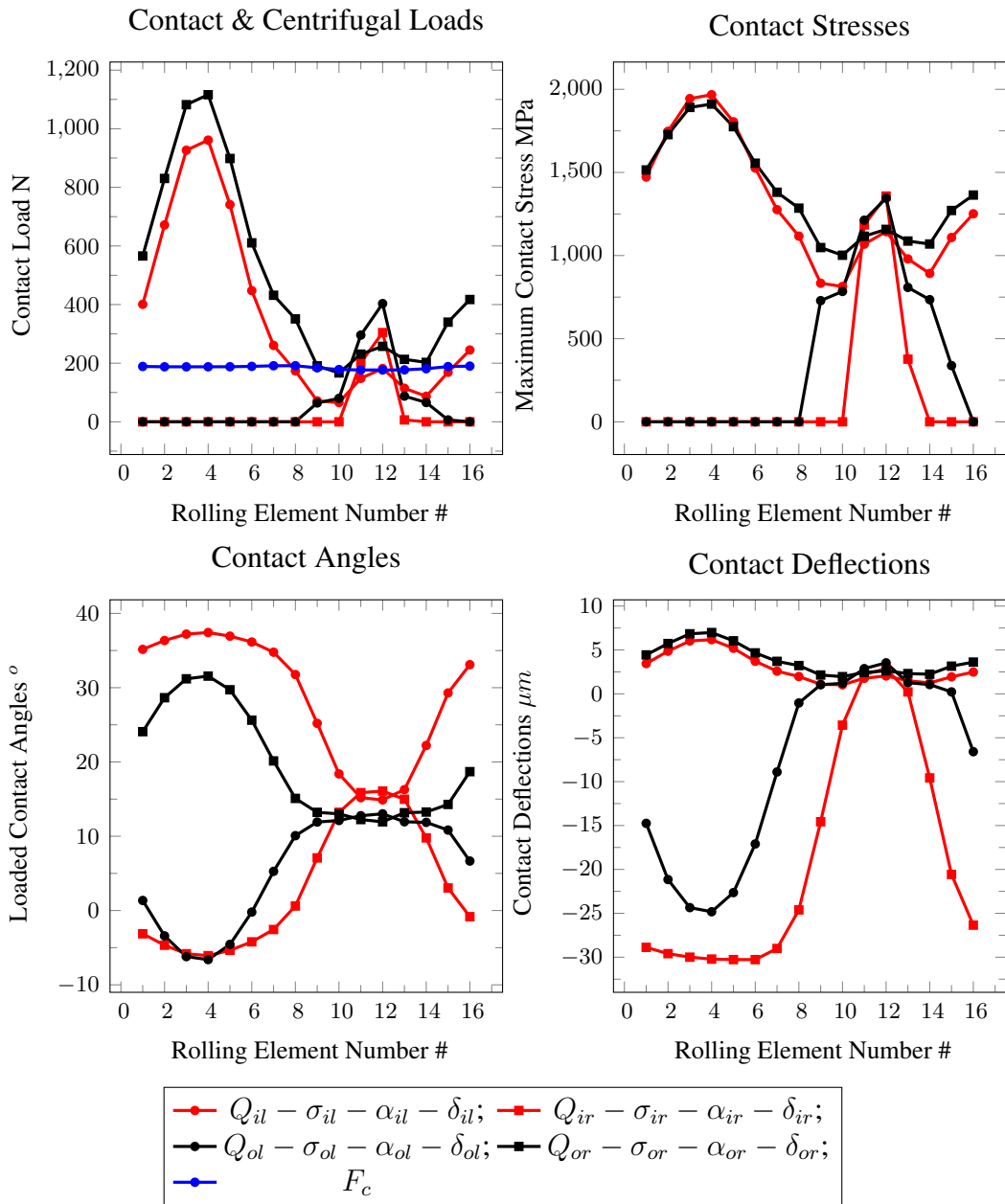


Figure 3.10: Results for Load C

### 3.8 Validation of the Model with FEA & CalyX Software

In this section established mathematical model for load distribution is compared with the finite element solutions. For this purpose, CalyX software is utilized. Also, comparison with the recent study [16] that simulates the four-point contact slewing bearing with FEA tool is given.

#### 3.8.1 Comparison with CalyX Software

CalyX is a computer program meant for the contact analysis of two- and three-dimensional multibody systems. It is a widely used tool in transmission design and analysis.

The 4PCBB geometry given in Table 3.2 is employed for the comparison. However, it is not possible to model the exact geometry of this 4PCBB in CalyX software. Therefore, Load A is selected for simulation in order to make this 4PCBB to act like an ACBB. Thus, the corresponding ACBB geometry, is modeled in the CalyX as an output shaft bearing of a simple one stage gearbox given in Figure 3.11.

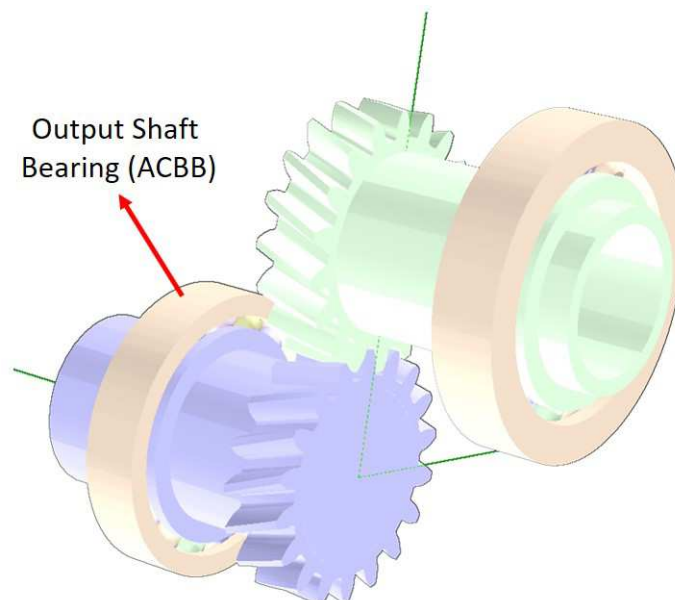


Figure 3.11: CalyX Gearbox Model for Validation

In order to control the load on the output shaft bearing, the torque in the system is set to an infinitesimal value which results approximately zero mesh loads induced on the bearing. The loading is applied to the output shaft which is the Load A given in Table 3.1. However, the centrifugal effects are not simulated in CalyX model, and in the MATLAB model the shaft speed is given as 0 rpm. The finite element meshed model of the system is given in Figure 3.12. As seen from this figure, the output shaft bearing is modeled with finer meshes.

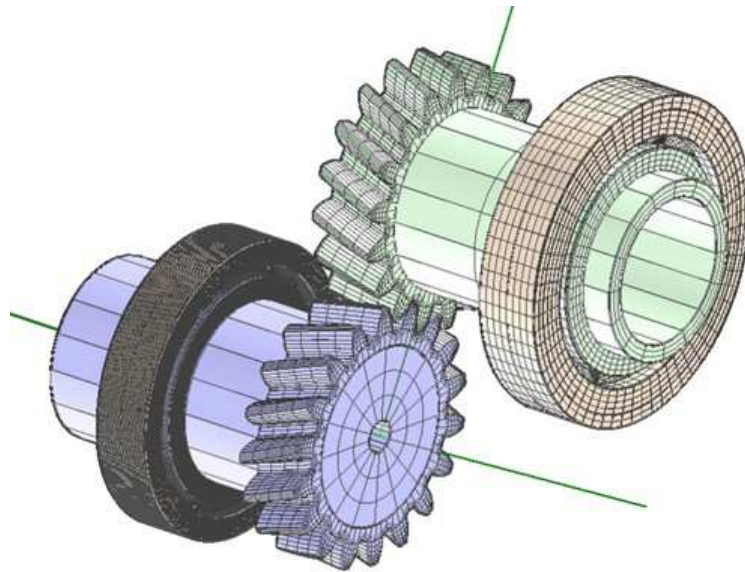


Figure 3.12: Simulation Results on Meshed Model

The other results that show the load distribution as well as the maximum contact stresses are given in Figure 3.13 and 3.14, respectively. Furthermore, the applied inner ring load and the bearing reaction force is given in that figure as a vector in pink color.

Since there is no centrifugal effects on both Calyx and MATLAB model, the loads for inner and outer raceways become equal and are compared in Figure 3.15 as contact load,  $Q$ . As it is seen from Figure 3.15, the load distributions are very similar.

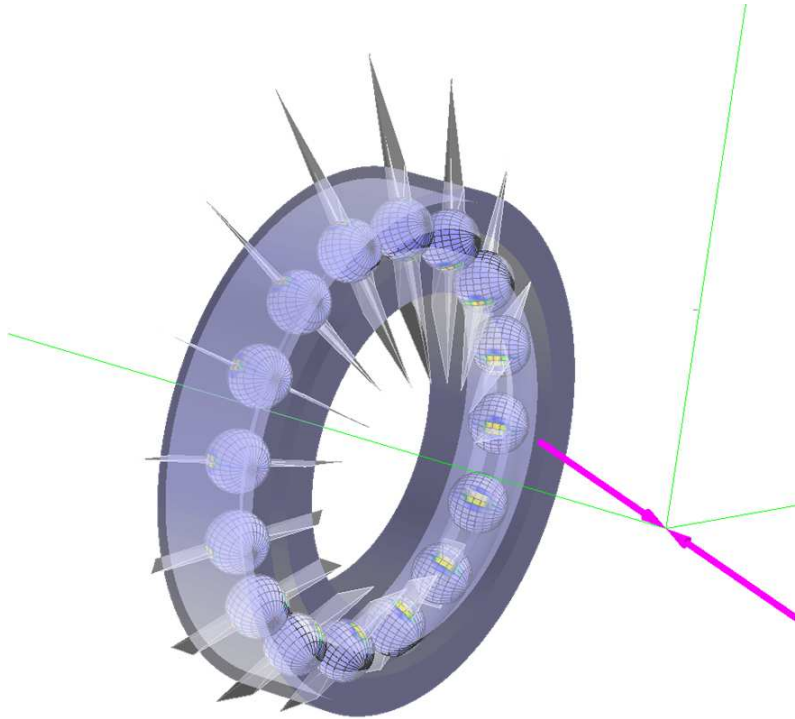


Figure 3.13: CalyX Load Distribution with Reaction Force

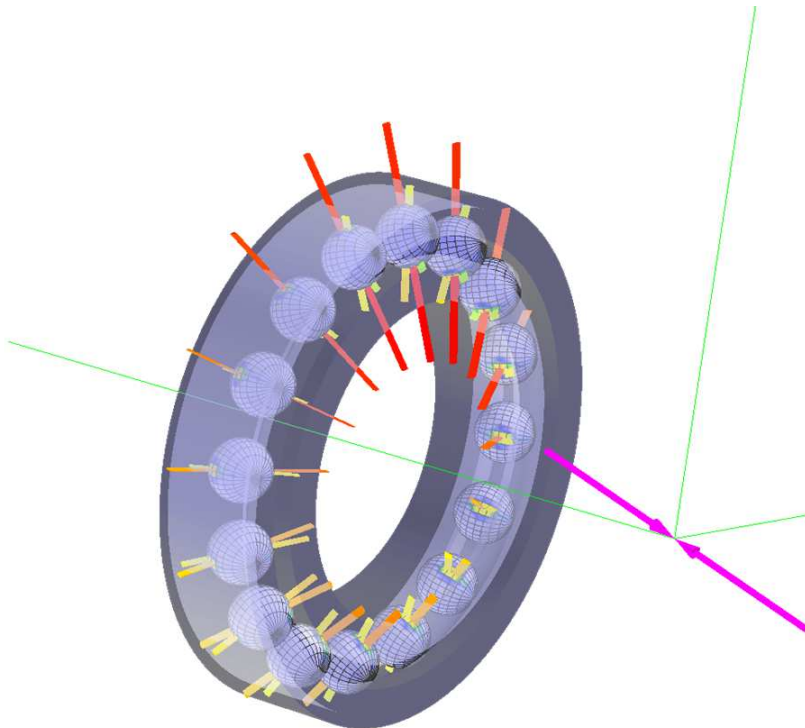


Figure 3.14: CalyX Maximum Contact Stress Distribution with Reaction Force

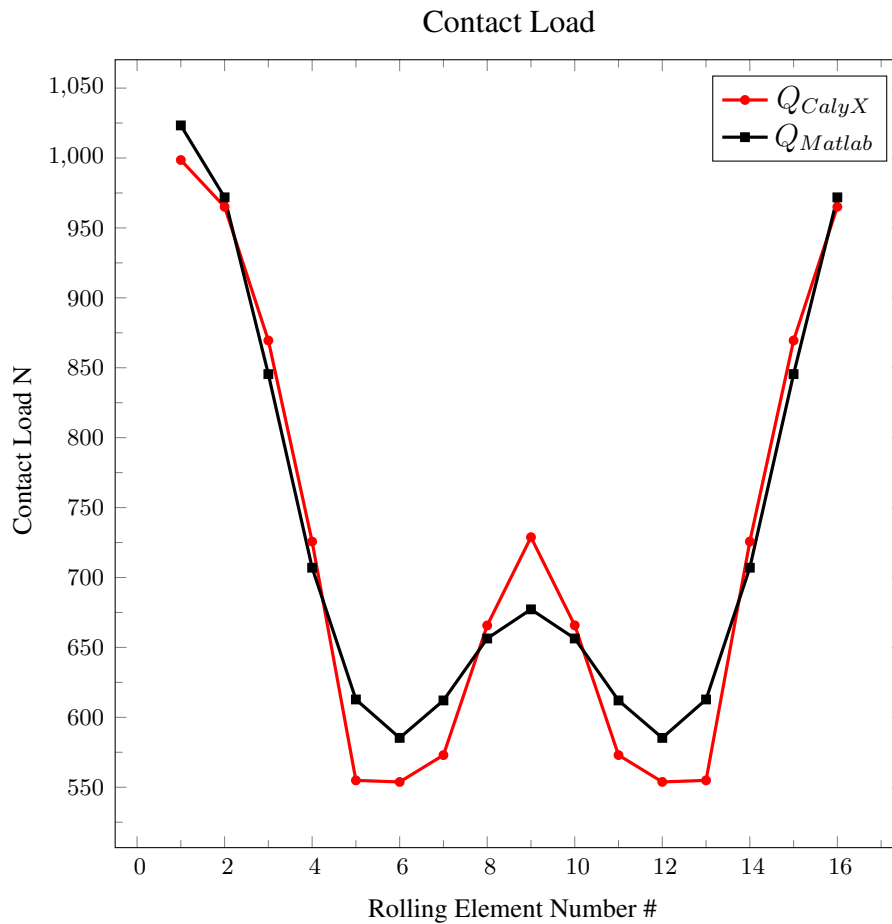


Figure 3.15: Contact Load Comparison of Calyx and MATLAB Model

The detailed numerical comparison is given in Table 3.3. The maximum error in the ball load is % 10.5 which is in the rolling elements 4 and 13. As it is seen from the comparison figure and table, the load distribution over the rolling elements are nearly same. The difference in the load values are due to the mesh size. In the Calyx model, it is observed that the mesh size is very effective on the results. However, with finer meshes the required simulation time becomes very high. Therefore, an average mesh size is selected for the simulation and comparison. Thus, with a finer meshed model, these differences shall be dramatically decreased.

Table 3.3: Numerical Comparison with CalyX Results

Ball Number	$Q_{CalyX}$ [N]	$Q_{Matlab}$ [N]	Error [%]
1	998.6	1023.3	2.5
2	965.1	971.9	0.7
3	869.5	845.4	-2.8
4	725.7	707.0	-2.6
5	554.9	612.8	10.4
6	553.8	585.3	5.7
7	573.0	612.1	6.8
8	665.7	656.4	-1.4
9	728.8	677.2	-7.1
10	665.8	656.4	-1.4
11	573.0	612.1	6.8
12	553.8	585.3	5.7
13	554.9	612.8	10.4
14	725.7	707.0	-2.6
15	869.5	845.4	-2.8
16	965.1	971.9	0.7

### 3.8.2 Comparison with Slewing Bearing Simulation Study in ABAQUS

Liu et al. [16] built a FE model for a single-row four-point-contact slewing bearing in ABAQUS software. The key to the method is to simulate the balls under compression by traction-only nonlinear springs. Furthermore, in the study, the comparison between numerical and experimental results are discussed in detail.

The model of the contact that Liu et al. incorporated for the study is given in Figure 3.16. As it is seen from this figure, traction-only non-linear springs are located between the raceway centers. The rigid shell and rigid beam elements are used to tie the raceways. By this way, the contact zones in the raceways are coupled with the corresponding raceway centers.

The four-point contact slewing bearing geometrical parameters for the study of Liu et al. [16] is given in Table 3.4.

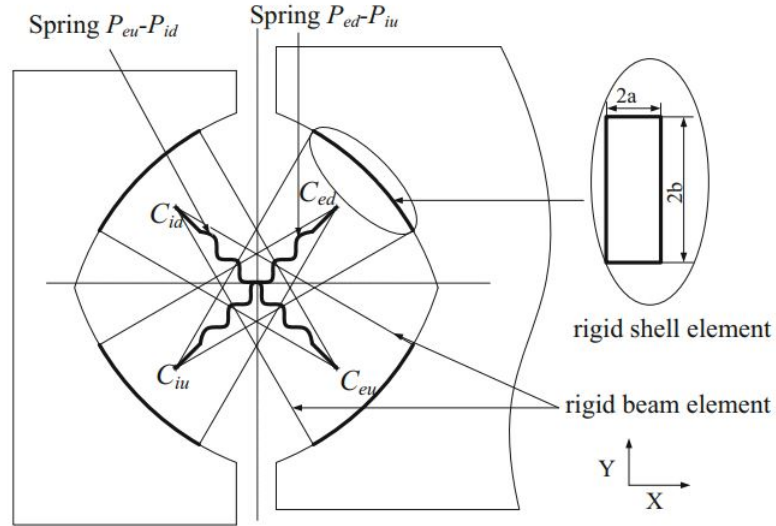


Figure 3.16: Model of the Contact [16]

Table 3.4: Geometrical Parameters of the Slewing Bearing [16]

	Value	Unit
$d_m$	1000	mm
$D$	40	mm
$Z$	69	#
$f_i$	0.525	-
$f_o$	0.525	-
$r_i$	21	mm
$r_o$	21	mm
$g_i$	1.414	mm
$g_o$	1.414	mm
$\alpha_{si}$	45	$^\circ$
$\alpha_{so}$	45	$^\circ$
$\alpha_0$	45	$^\circ$
$R_i$	500.707	mm
$R_o$	499.203	mm

The corresponding FE model for these geometrical parameters are given in Figure 3.17. As it is seen from the figure, the boundary conditions for symmetry are employed. Therefore, only half of the bearing as well as half of the total number of rolling elements are analyzed. Moreover, the coordinate frame for the bearing loads

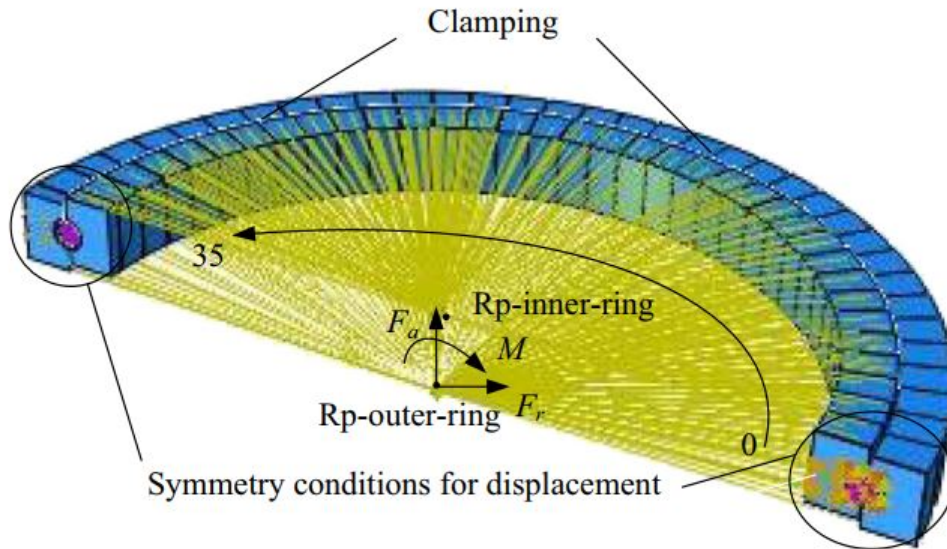


Figure 3.17: FE Model of the Slewing Bearing [2]

are given in Figure 3.17.

Liu et al. simulate the slewing bearing under several load levels. In these loadings only the axial and moment loads are applied. Thus, load distribution result for a specific load level is presented in detail. This load level is given as;  $F_a = 91.5$  kN  $M = 216.5$  kN.m. For coordinate frame of the 4PCBB model that is given in this study, this load level corresponds to the following load combination;  $F_x = 0$  kN,  $F_y = 0$  kN,  $F_z = 91.5$  kN,  $M_x = 0$  kN.m and  $M_y = -216.5$  kN.m. Since the centrifugal effects are disregarded, the shaft speed is taken as zero in MATLAB model. As a result, the contact loads for inner and outer raceways become equal such as;  $Q_{il} = Q_{or}$  and  $Q_{ir} = Q_{ol}$ .

The load distribution obtained in Liu's study [16] is given in the Figure 3.18. Spring Peu-Pid corresponds to the spring between the left inner and right outer raceway centers. Similarly, spring Ped-Piu corresponds to the spring between the right inner and left outer raceway centers.

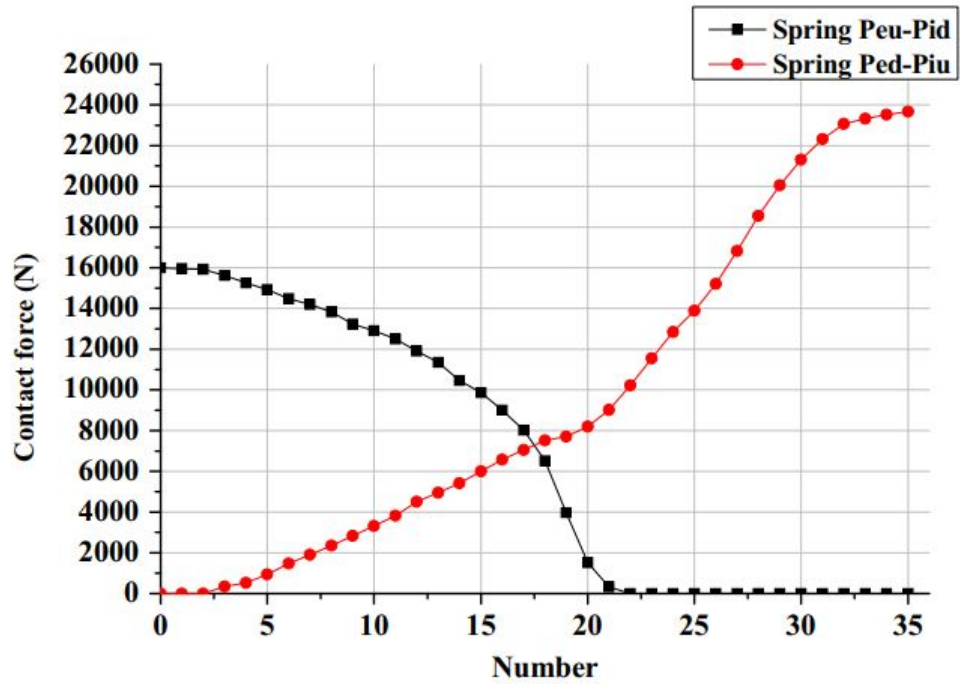


Figure 3.18: Load Distribution of the Slewing Bearing [16]

Resulting load distribution is obtained as given in Figure 3.19 with the established MATLAB model. In Figure 3.19, the FEA results are also illustrated in order to see the differences and similarities between these two models. Load distribution trends are similar for these two models. However, considerable differences occur in the contact load results of rolling elements from number 5 to number 21. In Liu's model [16] both springs are active and the rolling elements (# 5 to # 21) are loaded in four-point contacts. This situation is not observed in the MATLAB model results. This difference is due to the flexibility of the rings that is included in FE model but excluded in MATLAB model.

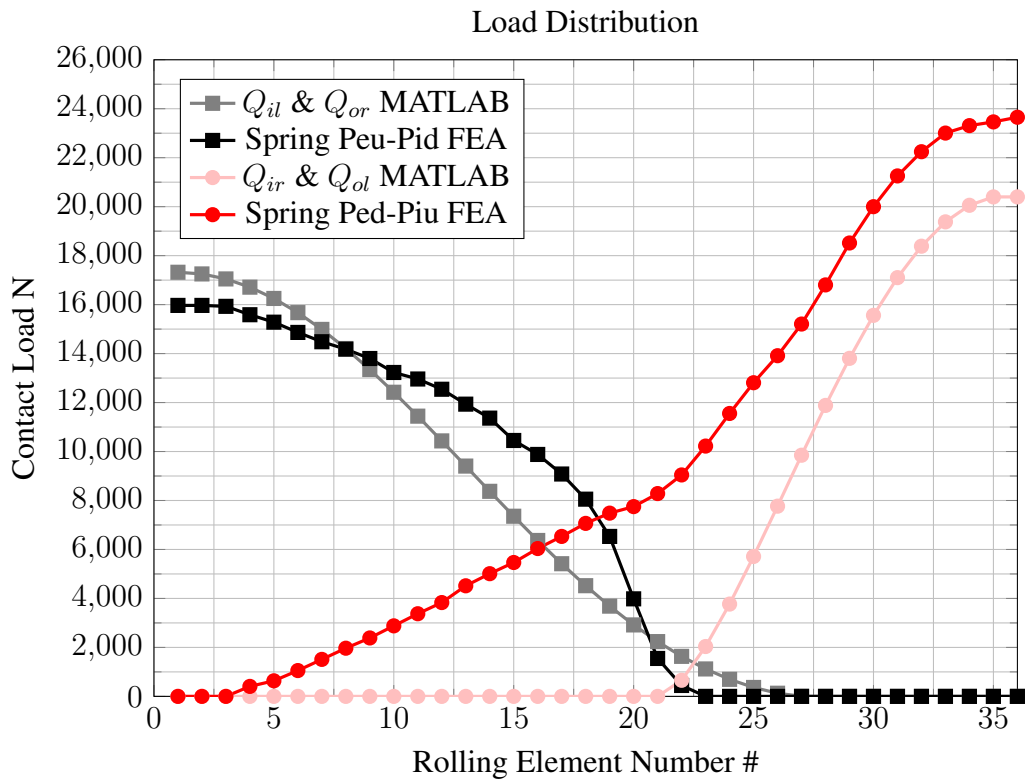


Figure 3.19: Load Distribution Comparison of FEA and MATLAB Models

Both comparisons with the CalyX and the Liu's study give enough precision in terms of the load distribution. After verifying the MATLAB model with both CalyX and a FEA study, the model is employed for the optimization subroutine.

## CHAPTER 4

### MICRO GEOMETRY OPTIMIZATION OF 4PCBB

In this chapter, the established optimization subroutine is presented in terms of the fixed parameters & design variables, constraints and the objective function to be minimized. In addition, optimization algorithm is basically described. Sample results that obtained with the micro-geometry optimization and discussions over these results are also presented at the end of this chapter.

#### 4.1 Optimization Algorithm

For optimization purpose, MATLAB software is utilized as in the load distribution model. Existing optimization solver in MATLAB; "fmincon" is employed for optimization. In this optimization solver, boundaries for design variables are introduced. These boundaries are described in following sections for each design variables. Moreover, the constraints that must be satisfied within the optimization are also stated and the implementation is given in the following sections. Optimization solver "fmincon" uses the "interior-point" algorithm in default. "interior-point" handles large, sparse problems, as well as small dense problems. The algorithm satisfies bounds at all iterations, and can recover from "Not a Number (NaN)" or infinite results. The algorithm can use special techniques for large-scale problems. Therefore, the default algorithm; "interior-point" is utilized for the optimization purpose.

The load distribution model including the post-process calculations are formed as a function,  $f_{4PCBB}$  in a MATLAB script. This function has the input and output

parameters which are given as in Equation 4.1.

$$\left| \begin{array}{l} d_m, D, Z, St_i, St_o, S_d \\ f_i, f_o, g_i, g_o \\ F, \omega \end{array} \right| \Rightarrow f_{4PCBB} \Rightarrow \left| \begin{array}{l} \delta \\ Q_{mk,j}, F_{c,j}, \alpha_{mk,j}, \delta_{mk,j} \\ \sigma_{mk,j}, TR_{mk,j} \end{array} \right| \quad (4.1)$$

By using  $f_{4PCBB}$  function in an optimization loop, design variables are optimized. Selection of the design variables as well as the fixed parameters are given in following section.

## 4.2 Fixed Parameters & Design Variables

In this section selected fixed parameters and the optimization design variables are introduced. The optimization is focused on the micro geometry of a custom design 4PCBB under a specific load and speed condition. Therefore, the macro geometrical parameters are selected as fixed parameters.

In the rotating machinery applications, there exist many constraints that designer shall obey in rolling element bearing design such as: shaft diameter, housing diameter. For this reason, optimization of the macro geometry of a custom design 4PCBB is out of scope for this study. To illustrate, bore diameter,  $D_i$  and outer diameter,  $D_o$  of the bearing is dependent on the available space within the design. Bearing pitch diameter,  $d_m$  and ball diameter,  $D$  are also needed to be selected with respect to the bore and outer diameter. In addition, in the industry it is not possible to find rolling elements with any diameters. These ball diameters are standardized by the manufacturer. Therefore, optimization of these ball diameter is not feasible. Once these parameters are selected, the cage design is another constraint that indicates the maximum number of balls,  $Z$  which can be employed for this specific design. Shoulder thicknesses,  $St_i$ ,  $St_o$  are also fixed and not included in optimization loop.

All parameters that are assumed to be pre-defined by the means of manufacturing, assembly easiness as well as the optimization efficiency are tabulated in Table 4.1. In this table, the design variables that optimized in terms of minimum contact stress and ellipse truncation are also given.

Table 4.1: Fixed Parameters & Design Variables

Fixed Parameters	Design Variables
$d_m$	
$D$	$f_i$
$Z$	$f_o$
$St_i$	$g_i$
$St_o$	$g_o$
$F$	$S_d$
$\omega$	

The design variables consist the osculation of inner and outer raceways,  $f_i$ ,  $f_o$  as well as the shim thicknesses for inner and outer rings,  $g_i$ ,  $g_o$ . Moreover, non-arched radial clearance,  $S_d$  is also optimized within the optimization subroutine. These design variables are the micro geometrical features of the custom design 4PCBB which indicates the unloaded contact angle,  $\alpha_0$  with the other fixed parameters. Therefore, the axial load carrying capacity, radial clearance, axial clearance and the other characteristics which are effective on the maximum contact stress, ellipse truncation as well as the four point contact behaviour are very much dependent on the bearing micro geometry. In the bearing design, optimization of these parameters is highly important and make the bearing to operate more efficiently for a selected application.

### 4.3 Constraint Implementation and Objective Function of the Optimization

For the optimization, it is necessary to set boundaries for the selected design variables in order to stay in feasible region. In other words, for the sake of efficient and rational optimization, the design variables are constrained to be in a pre-determined interval. To illustrate, raceway osculations are usually in the limits of  $0.51 \geq f_{i,o} \leq 0.53$  in the bearing literature and manufacturing. Therefore, these limits are embedded into the optimization loop. Furthermore, the shim thicknesses,  $g_i$  and  $g_o$  are also limited in an interval by limiting the resultant shim angles,  $\alpha_{si}$  and  $\alpha_{so}$  in between  $5^\circ$  to  $45^\circ$  which is the general boundaries within bearing manufacturing. It is obvious that

higher shim angles than  $45^\circ$  would result a higher clearance drop  $(\Delta P_d)_i$  and  $(\Delta P_d)_o$  from Equations 2.13 and 2.14. The non-arched radial clearance  $S_d$  is also limited in an interval which assures that the arched radial clearance as well as the axial end-play is positive ( $P_d, P_e > 0$ ). However, the constraint that radial and axial clearance to be positive cannot be assured %100 percent by only employing boundaries to the non-arched radial clearance,  $S_d$ . Because the radial clearance drops,  $(\Delta P_d)_i$  and  $(\Delta P_d)_o$  and the axial end-play,  $P_e$  dependent on the other design variables ( $f_i, f_o, g_i, g_o$ ) as well as the boundaries of these design variables. In other words, limiting  $S_d$  in a very conservative way to assure positive radial and axial end-play for all  $f_i, f_o, g_i, g_o$  in the limits will result a very narrow interval for  $S_d$  which makes the optimization inefficient. Therefore, the positive axial end-play requirement is embedded not only by boundary implementation but also constraint implementation. In order to satisfy the axial end-play to be positive, Equations from 2.10 to 2.16 are rewritten in terms of the design variables to obtain Equation 4.5.

$$P_e = 2BD \sin \alpha_0 - g_i - g_o \quad (4.2)$$

$$= 2BD \sin \left[ \cos^{-1} \left( 1 - \frac{P_d}{2BD} \right) \right] - g_i - g_o \quad (4.3)$$

$$= 2BD \sin \left[ \cos^{-1} \left( 1 - \frac{S_d - (\Delta P_d)_i - (\Delta P_d)_o}{2BD} \right) \right] - g_i - g_o \quad (4.4)$$

Equation 4.4 is rewritten to control  $S_d$ , in order  $P_e$  to be positive, and following inequality, Equation 4.5 is obtained.

$$S_d > 2BD \left\{ 1 - \cos \left[ \sin^{-1} \left( \frac{g_i + g_o}{2BD} \right) \right] \right\} + (\Delta P_d)_i + (\Delta P_d)_o \quad (4.5)$$

In addition to, the upper limit for non-arched radial clearance,  $S_d$  is determined by fixing maximum unloaded contact angle  $\alpha_0$  to  $45^\circ$ . This is a general acceptable limit for the ACBBS, and applied to 4PCBBs. The inequality that satisfies this condition is derived in Equations from 4.6 to 4.9.

$$45^\circ > \cos^{-1} \left( 1 - \frac{P_d}{2BD} \right) \quad (4.6)$$

$$45^\circ > \cos^{-1} \left( 1 - \frac{S_d - (\Delta P_d)_i - (\Delta P_d)_o}{2BD} \right) \quad (4.7)$$

$$\cos 45^\circ < \left( 1 - \frac{S_d - (\Delta P_d)_i - (\Delta P_d)_o}{2BD} \right) \quad (4.8)$$

$$S_d < 2BD(1 - \cos 45^\circ) + (\Delta P_d)_i + (\Delta P_d)_o \quad (4.9)$$

Finally, the boundaries of  $S_d$  are formulated in terms of other design variables. For this purpose, the boundaries of  $f_i$ ,  $f_o$ ,  $g_i$ ,  $g_o$  are used in a way that the range of  $S_d$  is maximized but not narrowed. Formulation of boundaries for the design variables are given in Table 4.2.

Table 4.2: Boundaries for the Design Variables

Variable	Boundaries	
$f_i$	$f_{i,min} = 0.51$	$f_{i,max} = 0.53$
$f_o$	$f_{o,min} = 0.51$	$f_{o,max} = 0.53$
$g_i$	$g_{i,min} = (2f_{i,min}D - D) \sin 5^\circ$	$g_{i,max} = (2f_{i,max}D - D) \sin 45^\circ$
$g_o$	$g_{o,min} = (2f_{o,min}D - D) \sin 5^\circ$	$g_{o,max} = (2f_{o,max}D - D) \sin 45^\circ$
$S_d$	$S_{d,min} = \text{See Equation 4.5 with } f_{i,min}, f_{o,min}, g_{i,min}, g_{o,min}$	
	$S_{d,max} = \text{See Equation 4.9 with } f_{i,max}, f_{o,max}, g_{i,max}, g_{o,max}$	

After the formulation of the boundaries for the design variables, these boundaries are embedded into the "fmincon" solver as an input before the optimization starts. Thus, the optimization seeks the best solution in a predetermined and feasible region. Moreover, there exist other constraints than the optimization boundary. Namely, these constraints aim to avoid four point contact, truncation and negative end play within the optimized bearing micro geometry. These constraints are implemented by using the penalty functions with static penalty parameters. These penalty functions including the penalty parameters are added on the objective function,  $\phi(x)$ . Thus, the

constrained objective function of the optimization,  $\phi_c(x)$  is given as in Equation 4.10.

$$\phi_c(x) = \phi(x) + \sum_{s=1}^{N_p} W_s P_s(x) \quad \text{with } x = \begin{bmatrix} f_i \\ f_o \\ g_i \\ g_o \\ S_d \end{bmatrix} \quad (4.10)$$

Where  $\phi(x)$  is the unconstrained objective function which is simply the maximum contact stress over the bearing, and output of the  $f_{4PCBB}$ . Penalty functions,  $P_s$  multiplication with the penalty coefficients,  $W_s$  are added to the  $\phi(x)$  with  $s = 1, 2 \dots N_p$ . Where  $N_p$  is the total number of the penalty functions in other words the total number of constraints. These penalty functions are given in Equations from 4.11 to 4.17.

$$P_1 = \max(\sigma_{ir,j}) \quad (4.11)$$

$$P_2 = \max(\sigma_{ol,j}) \quad (4.12)$$

$$P_3 = \max(TR_{il,j}) \quad (4.13)$$

$$P_4 = \max(TR_{ir,j}) \quad (4.14)$$

$$P_5 = \max(TR_{ol,j}) \quad (4.15)$$

$$P_6 = \max(TR_{or,j}) \quad (4.16)$$

$$P_7 = \min(0, P_e)^2 \quad (4.17)$$

As seen from Equations 4.11 and 4.12, first two penalty functions are employed in order to avoid three or four point contact within any of the rolling elements. For this purpose, the raceways other than the primary raceways (inner-left and outer-right for an axial load in the direction +Z) are penalized in the case of contact stress occurrence in these secondary raceways. Namely, the maximum contact stresses over the rolling elements that located within the secondary raceways are taken for the penalization. The other penalty functions from  $P_2$  to  $P_6$  are utilized for the truncation avoidance while optimizing the micro-geometry. All contacts between each raceway and rolling element are analyzed for the truncation, and maximum truncation over the rolling

elements are selected for adding to the objective function for penalization. Finally, the last penalty function  $P_7$  is for positive axial end-play constraint. As seen from Equation 4.17, in the case of a negative axial end-play,  $P_7$  becomes positive. However, for the positive  $P_e$  values  $P_7$  is taken as zero which means no penalization applied.

#### 4.4 Optimization Results for Selected Bearing and Loading Conditions

In this section, results of the optimization that defined in previous sections are given for a selected bearing design and loading conditions. Moreover, the penalty coefficients as well as each iteration within the optimization subroutine are to be illustrated. For this purpose, the bearing design that is given in Table 3.2 is employed. However, as it is discussed earlier, the micro-geometry is to be optimized. Hence,  $f_i$ ,  $f_o$ ,  $g_i$ ,  $g_o$  and  $S_d$  parameters are going to be optimized for different loading conditions with different optimization objectives. In following subsections, these different objectives and optimization are to be illustrated for the bearing with same macro-geometry.

The penalty coefficients,  $W_s$  that define the weight of each penalty functions need to be selected according to the purpose of the optimization. To illustrate, it is possible for the optimization subroutine to end up with a design point which cannot achieve to satisfy all the constraints implemented by penalty method. Therefore, by arranging the weight of the penalty functions with the coefficients, it is possible to direct the optimization to a design point which is more closer to satisfy the preferred constraints. Therefore, these penalty coefficients are specifically selected for each optimization cases. Moreover, these parameters shall be suitably selected in order to have same order of magnitude within each penalty functions. In other words, since each penalty function has different units, the weights shall be selected accordingly. For example,  $P_1$  and  $P_2$  are contact stresses in MPa. In addition to, the penalties from  $P_3$  to  $P_6$  are the truncations in percentages. Lastly,  $P_7$  is the end-play in millimeters. Therefore, it is important to assign weights to these functions according to these units and possible function values for an efficient optimization.

#### 4.4.1 Optimization #1: Focusing On Four-Point Contact Avoidance

In this optimization case, bearing is optimized for a loading with low axial to radial load ratio (i.e.  $F_z/F_x = 1.5$ ) as given in Table 4.3. Namely, in the non-optimized bearing design given in Table 3.2, four point contact is observed under this load condition. Therefore, the optimization in this subsection focuses on avoiding four point contact by changing the micro-geometry of the bearing. Thus, both non-optimized and optimized bearing parameters as well as the resulting contact stress distributions are to be provided. For the optimization #1, penalty coefficients are selected such as:  $W_{1,2} = 10^2$ ,  $W_{3,4,5,6} = 10^3$  and  $W_7 = 10^6$ .

Table 4.3: Loads for the Optimization #1

	Load / Speed
$F_x$ [N]	2000
$F_y$ [N]	0
$F_z$ [N]	3000
$M_x$ [Nm]	0
$M_y$ [Nm]	0
$n$ [rpm]	23000

Optimization finds an optimum point which satisfies the constraints by minimizing the penalty functions as well as the maximum contact stress. In Figure 4.1, the constrained and non-constrained objective function evaluation during the optimization iterations are given. It is observed that the constrained and non-constrained objective functions are converged to be equal. It means that all the penalty functions become zero. In other words, all the constraints are satisfied when the values of constrained and non-constrained objective functions are same.

As it is seen from Table 4.4, it takes 7 iterations for optimization subroutine to reach the optimum point. The non-constrained objective function,  $\phi$  which is simply the maximum contact stress over all rolling elements and raceways are listed for each iterations. Obviously, maximum contact stress is increased from 1913.9 MPa to 2056.5 MPa. However, as it is seen from Figure 4.2 four point contact is avoided by the help of the optimization subroutine. To illustrate, initial micro-geometry results to have four point contact in some of the rolling elements, whereas in the optimized micro-

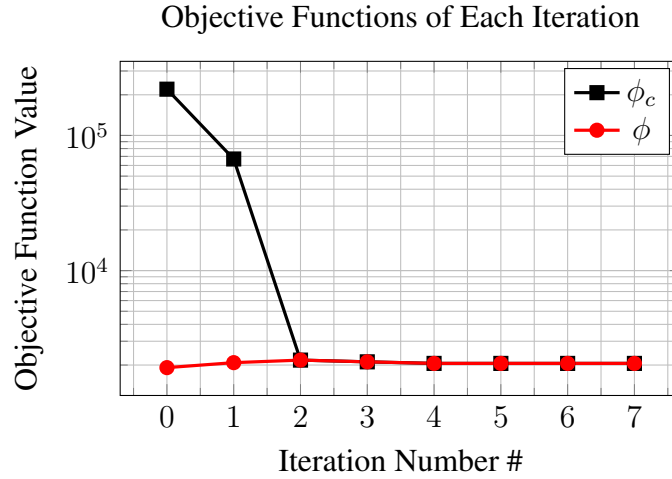


Figure 4.1: Objective Functions at Each Iteration of Optimization #1

Table 4.4: Iterations of Optimization #1

Iter.	Micro-geometrical Parameters					Non-const. Obj. Func.
	$f_i$	$f_o$	$g_i$	$g_o$	$S_d$	$\phi$
0	0.517	0.521	0.095	0.095	0.087	1913.9
1	0.519183	0.522511	0.082056	0.082056	0.19429	2083.1
2	0.524483	0.526181	0.050663	0.050663	0.123445	2175.7
3	0.522049	0.525443	0.045171	0.045171	0.103226	2112.6
4	0.520024	0.522847	0.040602	0.057869	0.086404	2056.7
5	0.520016	0.522837	0.040584	0.057919	0.086338	2056.5
6	0.520016	0.522837	0.040583	0.057922	0.086334	2056.5
7	0.520016	0.522837	0.040583	0.057922	0.086334	2056.5

geometry design the secondary raceways (inner-right and outer-left) and balls have no contacts as given in Figure 4.2. When it is compared with the excess heat generation as well as the premature failure due to this four point contact, contact stress increase in the amount of  $\sim 7.5\%$  is way better than acceptable.

In the Optimization # 1, it is aimed to optimize the bearing for preventing the four point contact in any of the rolling element. Therefore, the penalty coefficients,  $W_s$  are arranged accordingly. Thus, preventing of four point contact is achieved with small amount of increase in maximum contact stress. In the following subsections, other optimizations are to be carried out with different targets and geometries.

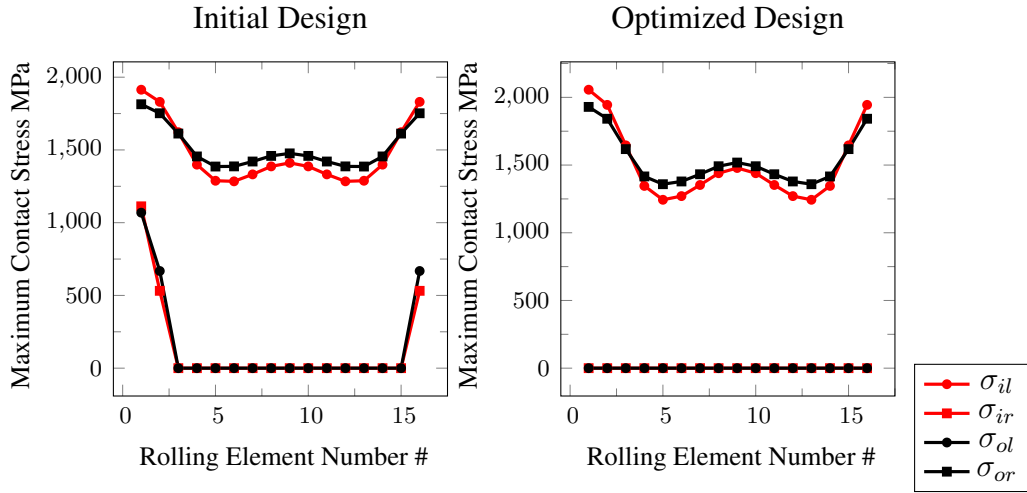


Figure 4.2: Contact Stress Distribution for Initial & Optimized Design of Optimization #1

#### 4.4.2 Optimization #2: Mainly Focusing on Contact Stress Minimization

In the Optimization #2, it is aimed to optimize the same bearing geometry in Optimization #1 which is given in Table 3.2 under the Load A given in Table 3.1. Previously, it is known that this bearing micro-geometry configuration under specified Load A acts like an ACBB which means no four point contact is observed. Thus, in this optimization, maximum contact stress of the bearing in any of the rolling element is aimed to be minimized. Like in the Optimization #1, non-optimized micro-geometry is given as an initial point for the iterations of the subroutine. By this way, the iterations shall converge to a more optimized bearing micro-geometry with lower contact stresses rather than the initial point micro-geometry.

In Figure 4.3, it is seen that the non-constrained and constrained objective functions,  $\phi$  and  $\phi_c$  are equal for all iterations which means no penalty is induced on the constrained objective function. In the optimization process, at each iteration algorithm searches for different points by calling multiple function evaluations and tends to the best point. Thus, design variables stay in the feasible region over the iterations because of the penalty functions. Design variables at each iteration as well as the maximum contact stresses are given in Table 4.5 in detail.

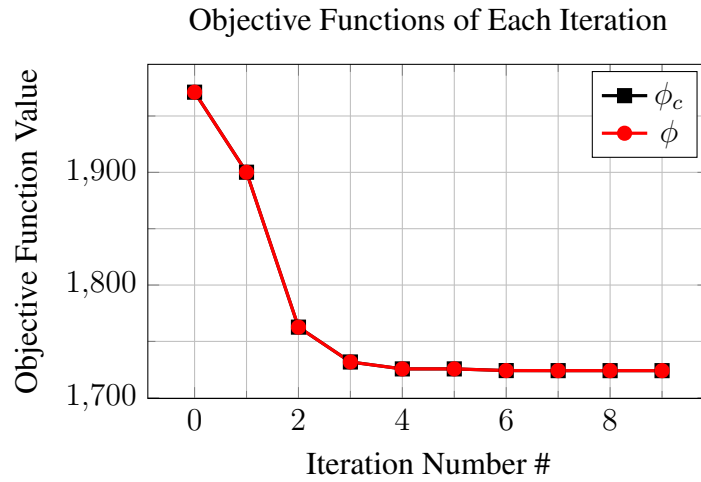


Figure 4.3: Objective Functions at Each Iteration of Optimization #2

As it is seen from Table 4.5, there is a decrease in the maximum contact stress by  $\sim 12.5\%$  from the non-optimized to optimized micro-geometry. Thus, the bearing is optimized in 9 iterations to have lower contact stress. Moreover, the initial and the final stress distributions of the bearing design under specified load is given in Figure 4.4.

Table 4.5: Iterations of Optimization #2

Iter. #	Micro-geometrical Parameters					Non-const. Obj. Func.
	$f_i$	$f_o$	$g_i$	$g_o$	$S_d$	$\phi$
0	0.517	0.521	0.095	0.095	0.087	1971.124
1	0.513570	0.515610	0.057264	0.057264	0.045909	1900.111
2	0.511071	0.511683	0.029770	0.029770	0.050008	1762.654
3	0.511017	0.510505	0.021522	0.021522	0.065841	1731.746
4	0.510933	0.510463	0.055804	0.055804	0.080514	1725.620
5	0.510933	0.510464	0.055817	0.055817	0.080515	1725.612
6	0.510915	0.510455	0.056602	0.055068	0.081225	1724.115
7	0.510915	0.510455	0.056587	0.055085	0.081263	1724.061
8	0.510915	0.510455	0.056589	0.055083	0.081266	1724.057
9	0.510915	0.510455	0.056589	0.055083	0.081266	1724.057

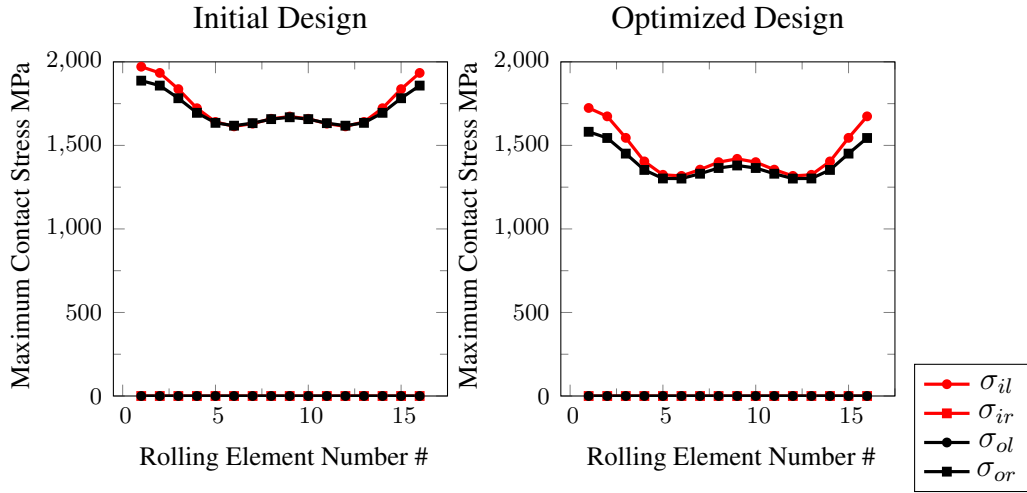


Figure 4.4: Contact Stress Distributions for Initial & Optimized Design of Optimization #2

#### 4.4.3 Optimization #3: Focusing on Truncation Avoidance

In this optimization case, it is aimed to optimize the bearing design for truncation issues. Cage designs of bearings dictate the feasible shoulder diameters. Therefore, it is not always possible to have large shoulder thicknesses in the bearings. Moreover, weight saving especially in aerospace applications is very important. Thus, optimization of the micro-geometry for small shoulder thicknesses for the target of zero truncation carries great importance. For this optimization purpose, the bearing design given in previous optimization cases is utilized. However, in order to show the power of the optimization algorithm, the shoulder thicknesses  $St_i$  and  $St_o$  are to be decreased to a critical value that results ellipse truncation in between several rolling elements and raceways. To illustrate, in previous optimization cases the ratio  $St/D$  is taken as 0.3 for both inner and outer shoulders. Thus, this value is decreased to 0.165 for  $St/D$  in Optimization #3. Since dominant axial load is the reason for balls to override through the raceway shoulders, high axial loading of 7500 N with small radial load of 1500 N is applied for this optimization case. Namely, the bearing with non-optimized micro-geometry results maximum truncation of %10.1 between 9<sup>th</sup> ball and inner-left raceway. This non-optimized configuration is supplied as initial guess for the iterations as in the previous optimization cases. Thus, the objective

functions of each iteration are obtained as in Figure 4.5.

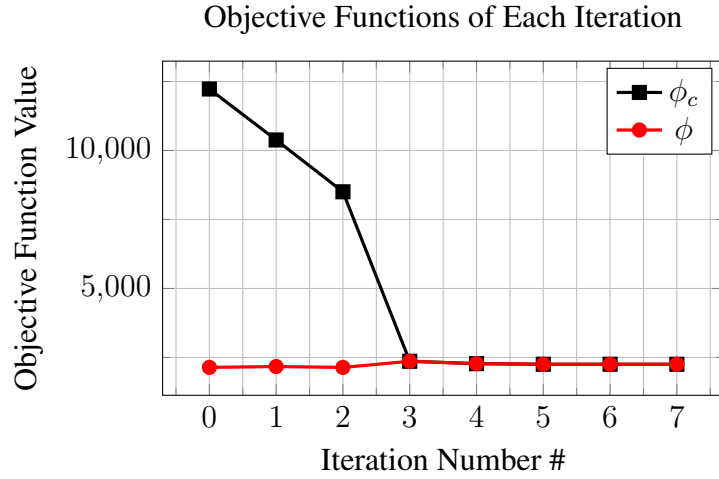


Figure 4.5: Objective Functions at Each Iteration of Optimization #3

As it is seen from Figure 4.5, constrained objective function,  $\phi_c$  converges to non-constrained one,  $\phi$  after three iterations. This implies that the penalty functions become zero after three iterations, and all the constraints are satisfied. Moreover, it is seen that the maximum contact stress is increased a little for the sake of satisfying the constraints. In Table 4.6, micro-geometrical parameters as well as the maximum contact stresses are listed for each iteration.

Table 4.6: Iterations of Optimization #3

Iter. #	Micro-geometrical Parameters					Non-const. Obj. Func.
	$f_i$	$f_o$	$g_i$	$g_o$	$S_d$	$\phi$
0	0.517	0.521	0.095	0.095	0.087	2140.917
1	0.516224	0.519713	0.085795	0.132469	0.076570	2170.550
2	0.516205	0.519715	0.085607	0.103992	0.076403	2138.734
3	0.522013	0.526381	0.090393	0.042788	0.059063	2361.959
4	0.518169	0.527171	0.091663	0.090160	0.059853	2275.773
5	0.517153	0.527243	0.091666	0.102261	0.059809	2253.683
6	0.517153	0.527243	0.091670	0.102261	0.059809	2253.675
7	0.517153	0.527243	0.091670	0.102261	0.059809	2253.675

As it is seen from Table 4.6, maximum contact stress within the rolling elements is increased from 2140.9 MPa to 2253.7 MPa, whereas no truncation is observed with the

optimized micro-geometry. Thus, the optimization reaches its target by eliminating any truncation within the bearing by changing the micro-geometry. Initial and optimized contact stress as well as the truncation distributions are illustrated in Figures 4.6 and 4.7, respectively.

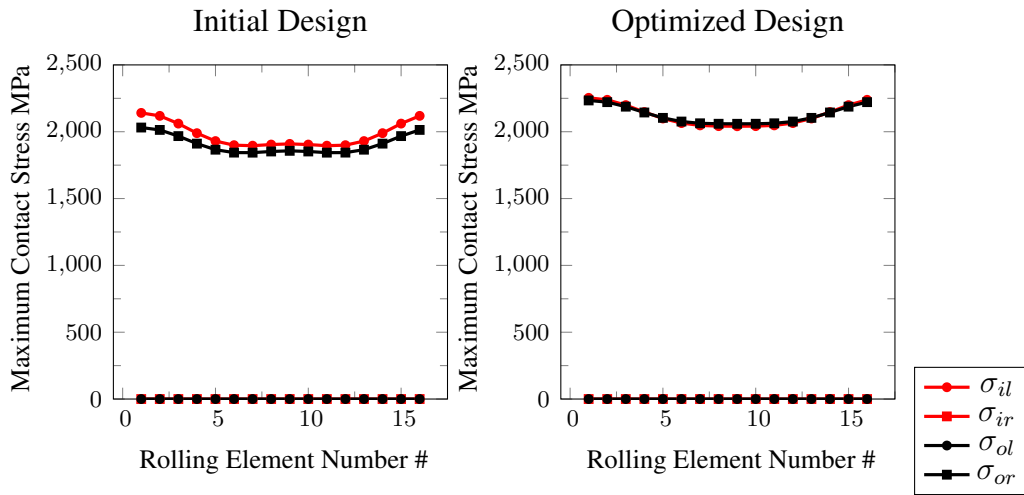


Figure 4.6: Contact Stress Distributions for Initial & Optimized Design of Optimization #3

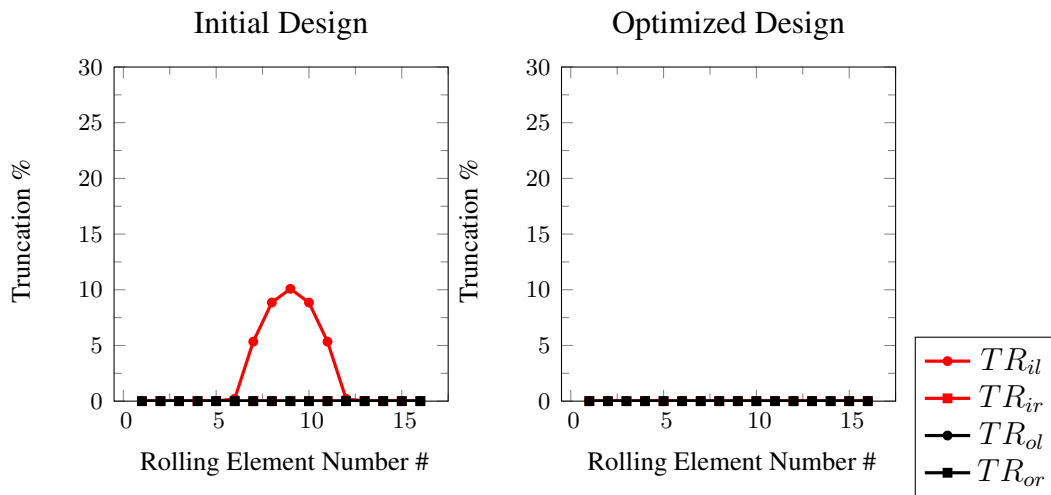


Figure 4.7: Truncation Distributions for Initial & Optimized Design of Optimization #3

## 4.5 Summary and Discussions over Optimization Results

In this section, results of the optimizations that carried out in the previous section are to be summarized and discussed. For this purpose, a general summary is provided in Table 4.7.

Table 4.7: Summary of the Optimizations

		Optimization #1	Optimization #2	Optimization #3
Macro-geo. Parameters	$d_m$	72.480 mm		
	$D$	10.319 mm		
	$Z$	16		
	$St_i/D$	0.3		0.165
	$St_o/D$	0.3		0.165
Initial Micro-geo. Parameters	$f_i$	0.517		
	$f_o$	0.521		
	$g_i$	0.095 mm		
	$g_o$	0.095 mm		
	$S_d$	0.087 mm		
Initial Pre-calculated Parameters	$\alpha_{si}$	15.710 °		
	$\alpha_{so}$	12.662 °		
	$P_d$	0.063 mm		
	$\alpha_0$	23.188 °		
	$P_e$	0.119 mm		
Loading Conditions	$F_x$	2000 N	1500 N	1500 N
	$F_y$	0 N	0 N	0 N
	$F_z$	3000 N	5000 N	7500 N
	$M_x$	0 Nm	0 Nm	0 Nm
	$M_y$	0 Nm	0 Nm	0 Nm
	$n$	23000 rpm	23000 rpm	23000 rpm
Penalty Coefficients	$W_s$	$W_{1,2} = 10^2$		$W_{1,2} = 10$
		$W_{3,4,5,6} = 10^3$		$W_{3,4,5,6} = 10^3$
		$W_7 = 10^6$		$W_7 = 10^6$
Initial Results	4PC ?*	YES	NO	NO
	$TR_{max}$	0 %	0 %	10.1 %
	$\sigma_{max}$	1913.9 MPa	1971.1 MPa	2140.9 MPa
Optimized Results	4PC ?*	NO	NO	NO
	$TR_{max}$	0 %	0 %	0 %
	$\sigma_{max}$	2056.5 MPa	1724.1 MPa	2253.7 MPa

\* Four Point Contact ?

Moreover, optimized bearing micro-geometry as well as the corresponding calculated geometrical parameters are given in Table 4.8.

Table 4.8: Optimized Geometrical Parameters

		Optimization #1	Optimization #2	Optimization #3
Optimized Micro-geo. Parameters	$f_i$	0.520016	0.510915	0.517153
	$f_o$	0.522837	0.510455	0.527243
	$g_i$	0.040583 mm	0.056589 mm	0.091670 mm
	$g_o$	0.057922 mm	0.055083 mm	0.102261 mm
	$S_d$	0.086334 mm	0.081266 mm	0.059809 mm
Optimized Pre-calculated Parameters	$\alpha_{si}$	5.638 °	14.549 °	15.008 °
	$\alpha_{so}$	7.059 °	14.790 °	10.479 °
	$P_d$	0.081 mm	0.067 mm	0.038 mm
	$\alpha_0$	24.676 °	31.970 °	16.637 °
	$P_e$	0.271 mm	0.122 mm	0.068 mm

In addition, computation time as well as the iterations that appear on the command window of MATLAB during the optimization process are given at Appendix A.1, A.2 and A.3 for Optimization #1, #2 and #3, respectively. In these command window results, function evaluation numbers are given in "F-count" column. These function evaluation numbers indicate how many times the function,  $f_{APCBB}$  is called out for each iteration.

In the Optimization #1, iterations altered the bearing micro-geometry such a way that in the final optimized design, there exist no three- or four-point contact loading in any of the rolling elements. This is achieved by decreasing the shim angles,  $\alpha_{si}$  and  $\alpha_{so}$  from  $15.710^\circ$  and  $12.662^\circ$  to  $5.638^\circ$  and  $7.059^\circ$ , respectively. Moreover, osculations,  $f_i$  and  $f_o$  are both increased in the small amount in order to guarantee the minimum contact stress after avoiding the four-point contact within the bearing. From these results it is observed that four-point contact tendency is related with the shim thicknesses,  $g$  and shim angles,  $\alpha_s$  with the combination of osculations. Thus, if the shim angles and shim thicknesses are increased, it is highly probable to witness four-point contact in the bearing even for a small amount of radial load. Therefore, in Optimization #1, algorithm alters the micro-geometry design to avoid the four-point contact by decreasing the shim angles and shim thicknesses. However, this procedure

is not possible to be applied for all applications. To illustrate, for this optimization the axial to radial load ratio is taken as  $F_z/F_x = 1.5$ . If this ratio is decreased to lower values, it may become impossible to generate a solution which both avoids four-point contact and satisfies the constraints of the optimization.

In the second optimization case, the bearing initially has no four-point contact in any rolling elements because of high  $F_z/F_x = 3.33$ . However, micro-geometry design results a maximum contact stress of  $\sigma_{max} = 1971.1$  MPa. Thus, by the help of optimization this contact stress is decreased to  $\sigma_{max} = 1724.1$  MPa. Since the optimization case is not very limited by the constraints and penalties of four-point contact and truncation avoidance, the algorithm can freely adjust the parameters to decrease the maximum contact stress. However, in Optimization #1, with low  $F_z/F_x$ , algorithm converged to a solution with higher contact stress but avoided four-point contact.

Finally, in the Optimization #3, the algorithm is limited by the design of the shoulder thickness i.e.  $St/D = 0.165$  and with high axial loading of  $F_z = 7500N$ . Therefore, in this optimization the maximum contact stress is again increased as in Optimization #1. However, ellipse truncation is prevented in any of the rolling elements. By decreasing the contact angle,  $\alpha_0$  from  $23.188^\circ$  to  $16.637^\circ$ , ellipse truncation is avoided by making contact in lower contact angles and making contact zone to be moved away from the edge of the raceways to the center of the raceway. Thus, axial load carrying capacity is decreased and the maximum contact stress is increased for high amount of axial loading. Nevertheless, both Optimizations #1 and #3 are successful since they manage to prevent possible important premature failures within the bearing due to four-point contact and ellipse truncation by changing the micro-geometry of the bearing.



## CHAPTER 5

### CONCLUSIONS & FUTURE WORK

#### 5.1 Conclusions

In this study, 4PCBB geometrical parameters and internal kinematics are investigated and compared with the conventional ACBB. Mathematical model for load distribution of 4PCBB is modelled in MATLAB environment based on the existing studies and models. In this model, bearing inner and outer rings are assumed to be rigid, and only deformations in the ball and raceway contacts are taken into consideration according to Hertz contact theory with numerical approximation method given in [5]. Moreover, left and right raceways are modelled and assumed to have same geometrical parameters. In this study, material of the rings and rolling elements are selected as steel. However, it is possible to input different materials for the rings and balls to the model. Thus, hybrid bearing designs with steel rings and ceramic balls can also be studied with generated model. Loading in 5 DoF and rotational speed is applied into the inner rings and outer rings are assumed to be stationary and grounded. Centrifugal body forces acting on the rolling elements are taken into account in order to simulate the centrifugal effects which become effective at high rotational speeds. The Hertzian contact stress and ellipse truncation formulations that are needed to evaluate the performance of the bearing are given. MATLAB function "fsolve" is employed as the solver of the established model. Resultant load, loaded contact angle, deflection and maximal contact stress distributions of several bearing designs under different load conditions are illustrated. Generated model is then compared with the existing FEA study and results of software called "CalyX". Both comparisons give enough precision in terms of the load distribution. After the validation of the model, it is

utilized for the micro-geometry optimization of 4PCBBs. In this optimization subroutine, the micro-geometrical parameters are selected as the design variables to be optimized. Several constraints and boundaries are introduced for an efficient and feasible optimization. For the optimization purpose, MATLAB function "fmincon" is employed in order to implement the boundaries of design variables. Furthermore, the static penalty method is used for the manually implementation of other constraints to the algorithm. Several optimization study is carried out for different loading conditions, and these results are summarized and discussed. Thus, micro-geometry design of a customized 4PCBB for a specific application is automated by the help of the established subroutine.

## 5.2 Outcome of Study & Recommendations for Future Work

Outcome of this study is to give guidance in customized bearing design by finding the optimum combination of micro-geometrical parameters for a minimum contact stress. By this way, it is possible to generate the optimum bearing micro-geometry for a specific application. The constraints and boundaries can be adjusted according to the need of the application. To illustrate, it is possible to limit the axial clearance,  $P_e$  to a critical value for the applications where this parameter is needed to be controlled. Moreover, the boundaries that are given for osculations,  $f_i$  and  $f_o$  can be narrowed or expanded depending on the manufacturing capabilities. To summarize, the efficiency of the generated mathematical model for the load distribution of 4PCBB makes it possible to be utilized in an optimization subroutine. Therefore, modifications can be made on the established optimization subroutine in order to investigate for different optimization targets with different constraints and boundaries.

Finally, the possible future works that may be constructed on this study are to be given as follows:

- Ring deformations may be embedded into load distribution model for the analysis of bearings which seat to thin section supports. By this way, it would be possible to optimize the bearing for this type of applications where the ring deformations are dominant and effective.

- Optimizing the bearing not only for single load case but for multiple load cases may be added to the optimization subroutine.
- Tribological aspects of the bearing may be investigated and embedded into the model in order to increase the number of performance evaluation criterion such as: film thickness, friction torque and power loss.
- By employing the generated model for a series of bearings with different macro- and micro-geometrical parameters as well as with different load cases, transition from acting like a conventional ACBB to having three- or four-point contact may be captured, and an empirical formula may be generated.



## REFERENCES

- [1] Evolution SKF. Four-point Contact Ball Bearings – Two In One. <http://evolution.skf.com/four-point-contact-ball-bearings-two-in-one/>. [Online; accessed 23-March-2018].
- [2] Tibet Makina. Single-Row Ball Bearings (Four Points Contact Bearings). <http://www.tibetmakina.com.tr/group/2/single-row-ball-bearings-four-points-contact-bearings>. [Online; accessed 24-March-2018].
- [3] Harris, T. A. and Kotzalas, M. N. *Rolling Bearing Analysis*, volume I. Taylor & Francis, 5<sup>th</sup> edition, 2007.
- [4] ISO/TS 16281:2008(E) : Rolling bearings – Methods for calculating the modified reference rating life for universally loaded bearings. Technical specification, International Organization for Standardization, Geneva, CH, June 2008.
- [5] Antoine, J-F., Visa, C., Sauvey, C., and Abba, G. Approximate analytical model for hertzian elliptical contact problems. *ASME, Journal of Tribology*, pages 660–664, 2006.
- [6] Jones, A. B. A general theory for elastically constrained ball and radial roller bearings under arbitrary load and speed conditions. *ASME, Journal of Basic Engineering*, pages 309–320, 1960.
- [7] Harris, T. A. and Broschard, J. Analysis of an improved planetary gear transmission bearing. *ASME, Journal of Basic Engineering*, pages 457–462, 1964.
- [8] De Mul, J. M., Vree, J. M., and Maas, D. A. Equilibrium and associated load distribution in ball and roller bearings loaded in five degrees of freedom while neglecting friction – Part I: General theory and application to ball bearings. *Transactions of the ASME*, pages 142–148, 1989.
- [9] Lim, T. C. and Singh, R. Vibration transmission through rolling element bearings, Part I: Bearing stiffness formulation. *Journal of Sound and Vibration*, pages 179–199, 1990.
- [10] Hernot, X., Sartor, M., and Guillot, J. Calculation of the stiffness matrix of angular contact ball bearings by using the analytical approach. *ASME, Journal of Mechanical Design*, pages 83–89, 2000.

- [11] Hamrock, B. J. and Anderson, W. J. Analysis of an arched outer-race ball bearing considering centrifugal forces. Technical report, NASA Technical Memorandum, 1972.
- [12] Hamrock, B. J. Ball motion and sliding friction in an arched outer race ball bearing. *ASME, Journal of Lubrication Technology*, pages 202–211, 1975.
- [13] Amasorrain, B. J., Sagartzazu X., and Damian J. Load distribution in a four contact-point slewing bearing. *Elsevier, Journal of Mechanism and Machine Theory*, pages 479–496, 2003.
- [14] Leblanc, A. and Nelias D. Ball motion and sliding friction in a four-contact-point ball bearing. *ASME, Journal of Tribology*, pages 801–808, 2007.
- [15] Halpin, J. A. and Tran, A. N. An analytical model of four-point contact rolling element ball bearings. *ASME, Journal of Tribology*, pages 1–13, 2016.
- [16] Liu, R., Wang, H., Pang, B. T., Gao, X. H., and Zong, H. Y. Load distribution calculation of a four-point-contact slewing bearing and its experimental verification. *SEM, The Society for Experimental Mechanics*, 2018.
- [17] Gündüz, A., Sarıbay, Z. B., and Yılmaz, S. An integrated model for performance optimization of aerospace bearings considering high-speed rotations and temperature variations. *JAHS, Journal of the American Helicopter Society*, pages 012004–1 to 012004–9, 2018.
- [18] ISO 281 : Rolling bearings – Dynamic load ratings and rating life. Technical specification, International Organization for Standardization, Geneva, CH, December 1990.

## APPENDIX A

### COMMAND WINDOWS OF MATLAB DURING OPTIMIZATION

#### A.1 Command Window of MATLAB during Optimization #1

```
Iter F-count          f(x) Feasibility  Steplength      Norm of First-order
      0         6    2.200309e+05  0.000e+00      1.681e-01      1.089e-01      4.161e+06
User objective function returned Inf; trying a new point...
      1        17    6.697874e+04  0.000e+00      1.681e-01      1.089e-01      8.058e+06
      2        25    2.175731e+03  0.000e+00      4.900e-01      8.386e-02      7.202e+05
      3        36    2.112560e+03  0.000e+00      1.681e-01      2.181e-02      7.218e+05
      4        47    2.056718e+03  0.000e+00      1.681e-01      2.182e-02      7.234e+05
      5        73    2.056491e+03  0.000e+00      7.979e-04      8.617e-05      7.234e+05
      6       107    2.056478e+03  0.000e+00      4.600e-05      4.963e-06      7.234e+05
      7       139    2.056478e+03  0.000e+00      1.104e-05      1.192e-06      7.234e+05

Local minimum possible. Constraints satisfied.

fmincon stopped because the size of the current step is less than
the default value of the step size tolerance and constraints are
satisfied to within the default value of the constraint tolerance.

<stopping criteria details>

Elapsed time is 1267.483861 seconds.
>>
```

## A.2 Command Window of MATLAB during Optimization #2

Iter	F-count	f(x)	Feasibility	Steplength	Norm of First-order step	optimality
0	6	1.971124e+03	0.000e+00			1.015e+06
1	14	1.900111e+03	0.000e+00	4.900e-01	6.766e-02	4.856e+05
2	21	1.762654e+03	0.000e+00	7.000e-01	3.937e-02	4.846e+05
3	28	1.731746e+03	0.000e+00	7.000e-01	1.970e-02	2.093e+05
User objective function returned complex; trying a new point...						
4	41	1.725620e+03	0.000e+00	8.235e-02	5.065e-02	1.480e+06
User objective function returned complex; trying a new point...						
5	76	1.725612e+03	0.000e+00	3.220e-05	1.747e-05	1.930e+05
6	93	1.724115e+03	0.000e+00	1.977e-02	1.296e-03	1.894e+05
7	121	1.724061e+03	0.000e+00	3.910e-04	4.388e-05	1.894e+05
8	155	1.724057e+03	0.000e+00	4.600e-05	3.795e-06	1.894e+05
9	187	1.724057e+03	0.000e+00	1.104e-05	1.016e-06	1.894e+05

Local minimum possible. Constraints satisfied.

fmincon stopped because the size of the current step is less than the default value of the step size tolerance and constraints are satisfied to within the default value of the constraint tolerance.

<stopping criteria details>

Elapsed time is 981.985979 seconds.

>>

### A.3 Command Window of MATLAB during Optimization #3

Iter	F-count	f(x)	Feasibility	First-order optimality	Norm of step
0	6	1.222884e+04	0.000e+00	1.341e+07	
Objective function returned complex; trying a new point...					
1	15	1.038142e+04	0.000e+00	1.841e+06	4.000e-02
2	23	8.503802e+03	0.000e+00	3.043e+06	2.848e-02
3	29	2.361959e+03	0.000e+00	6.274e+05	6.440e-02
4	36	2.275773e+03	0.000e+00	5.203e+05	4.756e-02
5	45	2.253683e+03	0.000e+00	1.161e+06	1.214e-02
6	56	2.253675e+03	0.000e+00	7.952e+05	3.935e-06
7	76	2.253675e+03	0.000e+00	8.114e+05	3.967e-09

Local minimum possible. Constraints satisfied.

fmincon stopped because the size of the current step is less than the default value of the step size tolerance and constraints are satisfied to within the default value of the constraint tolerance.

<stopping criteria details>

Elapsed time is 1163.064481 seconds.

>>



## **APPENDIX B**

### **FLOWCHART OF LOAD DISTRIBUTION MODEL**

## B.1 Flowchart of the Mathematical Model for the Load Distribution of 4PCBB

